DESIGN AND CHARACTERIZATION OF MATERIALS WITH MICROPHASE-SEPARATED SURFACE PATTERNS FOR SCREENING OSTEOBLAST RESPONSE TO ADHESION

A Dissertation
Presented to
The Academic Faculty

by

Gracy A. Wingkono

In Partial Fulfillment
of the Requirements for the Degree
Doctor of Philosophy in Chemical Engineering

Georgia Institute of Technology
August 2009

DESIGN AND CHARACTERIZATION OF MATERIALS WITH MICROPHASE-SEPARATED SURFACE PATTERNS FOR SCREENING OSTEOBLAST RESPONSE TO ADHESION

Approved by:

Dr. J. Carson Meredith, Advisor
School of Chemical and Biomolecular Engineering
Georgia Institute of Technology

Dr. Sham Navathe
College of Computing
Georgia Institute of Technology

Dr. Andrés J. García
School of Mechanical Engineering
Georgia Institute of Technology

Dr. Mark Prausnitz
School of Chemical and Biomolecular Engineering
Georgia Institute of Technology

Dr. William Koros
School of Chemical and Biomolecular Engineering
Georgia Institute of Technology

Dr. Joseph Schork
School of Chemical and Biomolecular Engineering
Georgia Institute of Technology

Date Approved: August 17, 2009

ACKNOWLEDGEMENTS

I would like to express my heartfelt thanks to God who has made everything possible.

My special thanks to Dr. Carson Meredith for his continuous guidance, patience, and support. I am very grateful to him for giving an endless inspiration throughout my whole time being his graduate student.

I would like to gratefully acknowledge Dr. Andrés J. García, Dr. Clifford Henderson and Dr. Christopher Jones along with their research groups for their help with Fluorescence Microscopy, FTIR and Ellipsometry.

I would like to thank Dr. Andrés J. García, Dr. William Koros, Dr. Carson Meredith, Dr. Sham Navathe, Dr. Mark Prausnitz, and Dr. Joseph Schork, for dedicating their valuable time to serve on my committee.

The Advanced Polymer Thin Films and Colloid Materials research group is an amazing group; I always enjoy the great experience of being a part of the group and working with such talented individuals. I want to thank all group members for all the help and discussions, creating such a wonderful atmosphere for research.

In particular, I wish to thank my Mom and Dad, Mami, Meity, and also my dear friends who have been the vessel of blessings in my life. A lot of things happened during my study; yet their continuous support and sincere care are never ending, and they had strengthened me through it all.

TABLE OF CONTENTS

LIST OF TABLES

LIST OF FIGURES

LIST OF SYMBOLS AND ABBREVIATIONS

•	Weight fraction of pure PCL in blend	%
•	Weight fraction of PCL in segmented copolymer PEG-PU-PCL	%
ECM	Extra-cellular Matrix	
h	Film thickness	• m
MDI	4,4 Methylene bis-phenyl diisocyanate	
PCL	Poly(•-caprolactone)	
PEG	Poly(ethylene glycol)	
PEG-U	Poly(ethylene glycol) crosslinked with urethane bonds	
PEG-U-PCL	Segmented copolymer, PEG and PCL crosslinked with urethane bonds	
PETA	Penta Erythritol Triacrylate	
PS	Poly(styrene)	
R	$R = perimeter^2/(4.\pi.area)$	
Ra	Roughness	nm
Si	Silicon	
T	Annealing temperature	^oC
Tg	Glass transition temperature	^oC
Tm	Melting point	^oC
TQ	Quenching temperature	^oC
VASE	Variable Angle Spectroscopic Ellipsometer	
X	Coating Distance measured from the initial blade position	mm
Y	Paint Distance	mm

SUMMARY

Combinatorial techniques have changed the paradigm of materials research by allowing efficient screening of complex materials problems with large, multidimensional parameter spaces. The focus of this thesis is to demonstrate combinatorial methods (CM) and high-throughput methods (HTM) applied to biomaterials design, characterization, and screening. In particular, this work focuses on screening the effects of biomaterial surface features on adherent bone cell cultures. Polymeric biomaterials were prepared on two-dimensional combinatorial libraries that systematically varied the size and shape of chemically-distinct microstructural patterns. These libraries were generated from blends of biodegradable polyurethanes and polyesters prepared with thickness, composition and temperature gradient techniques. Characterization and screening were performed with high-throughput optical and fluorescence microscopy. A unique advance of this work is the application of data mining techniques to identify the controlling structural features that affect cell behavior from among the myriad variety of metrics from the microscope images.

Libraries were designed to exhibit chemically-distinct cell-adhesive versus non-adhesive microstructural domains that improve library performance compared to previous implementations that had employed only modest chemical differences. Improving adhesive contrast should minimize combination of effects of chemistry and physical structure, making data interpretation simpler. To accomplish this, a method of blending and crosslinking cell-non-adhesive *poly(ethylene glycol) (PEG)* with cell-adhesive

poly(•-caprolactone) (PCL) was developed. The behavior of MC3T3-E1 osteoblast cells cultured on the PCL-PEG libraries were observed, equivalent to thousands of distinct chemistries and microstructures.

Cell spreading area, shape, and density upon adhesion on surface patterns are observed in this study. Characterization of the surface library and screening of surface physical properties via HTM and PCA show that cell density is sensitive to the physical distribution, shape, solidity, and orientation of the PCL and PEG domains. Correlation is shown between surface pattern descriptors and the subsequent cellular adhesion responses. Certain spacing and shapes in surface pattern are preferred to others for distinct cellular states; circular pattern favors apoptotic cells, while elongated patterns favor viable cells - for both cases, cells preferred anchoring themselves to surface patterns. However, the effect of surface pattern's solidity and area did not show any conclusive trend in this dataset. This might be due to the existence of correlation between solidity and eccentricity as described in Chapter 1. Further improvement in the surface pattern library generation is necessary for future studies.

The results from this study demonstrated the potentials of CM/HTS to be applied to exploratory studies involving complex systems in life sciences. This study accomplishes the goal to demonstrate the efficient screening and exploration of vast and complex dataset, extracting important and meaningful information to narrow down the future path of study in this field.

Further study aimed to tuning cellular responses via signals from surface cues will be necessary to examine the causal relationships beyond the observed correlations shown in this exploratory study. It is recommended for further studies to narrow down the range

for surface patterning around each of the three ‘activation’ ranges found in this study: apoptotic, viable, and one unknown state to be studied further. Different cellular-function staining methods will be necessary to be used in cellular imaging techniques in order to explore this unknown state further.

CHAPTER 1

INTRODUCTION

1.1. Background

The application of biodegradable materials in the medical field initially started with the introduction of resorbable sutures. Now this field has grown to encompass tissue engineering and other therapies. Tissue engineering itself has evolved from designing simple “biocompatible” scaffolds towards developing “bioactive” materials for controlling cellular and physiological responses [1-8].

Bioactive polymers are of interest for tissue engineering scaffolds that support and regulate key elements in cellular responses such as adhesion, growth and function of target cells. Studies have shown that both chemical and physical surface properties control those cellular response [3, 4, 9-16]. Hence, biomaterial design requires a thorough understanding of these chemical and physical surface features and their effects on cellular responses.

Many studies have focused on the surface chemical aspects of signaling. Various ways of modifying surface adhesiveness such as using different polymer or coating/grafting with certain functional groups have been explored. For example, the certain amino acid sequence RGD (arginine-glycine-aspartic acid) is recognized by cell membrane integrins and is often necessary for promoting cell adhesion in osteoblasts and fibroblastic cells [1-3, 9, 11, 12]. RGD is one of the known cell-adhesive domains of the naturally occurring extracellular matrix protein fibronectin produced by most of adherent cell lines for subsequent adhesion [11, 12, 17-22]. The importance of physical surface

features in biomaterial design has also been recognized for decades. The in vitro studies of mammalian cells cultured on micro-patterned substrates has made significant contributions to fundamental cellular biology, tissue engineering, and cell-based bioelectronics. It is now widely accepted that spatial control of cellular adhesion and growth is critically important in these fields [4, 5, 9, 23]. It has been reported that cellular shape and movement (traction and migration) respond to the substrate mechanical strength of the biomaterial structure. This is crucial in cases such as wound healing [24, 25].

It is already known that surface roughness, geometric spacing of adhesive and non-adhesive area, and surface mechanical properties can influence some adherent cellular properties [1, 5, 9, 15, 26-32]. Cell behavior and cell fate dependence on cellular shape and anchorage in fibroblast cells have been studied for more than two decades [4, 5, 9, 15, 23, 33-35]. The ratio of adhesive to non- adhesive area, their spacing, and dimensions have been shown to be geometric controls of cellular life and death [9]. Much of this research has been done with surface patterning techniques adopted from microelectronics used to create model surfaces with well-controlled resolved microstructures [4, 9, 11, 12, 23, 34].

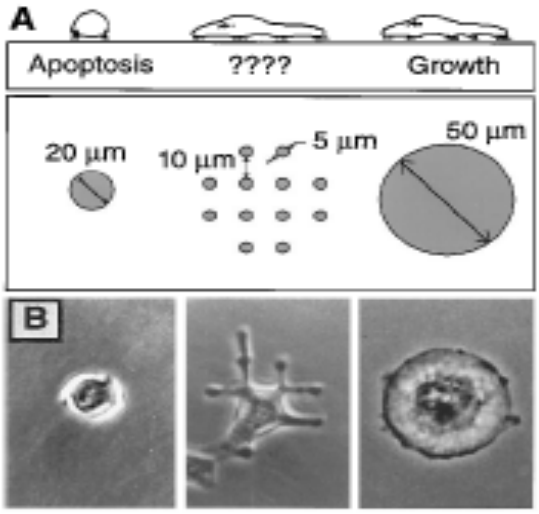

Figure 1. Model surfaces with well-controlled resolved microstructures [9]

However, physical microstructure and topography of applied biomaterials have not been explored nearly as much as their mechanical and chemical properties, despite their importance. Metals and various industrial plastics that are widely used for medical implants lack the molecular sequence and patterns crucial for normal cell function and therefore often trigger aberrant cell responses in longterm implantation [7]. Therefore more research linking chemical and physical surface properties with cell response are critical for future medical applications.

Major challenges in this scientific quest include the large number of parameters affecting applied biomaterial processing and synthesis. Scanning through the vast combinations of parameters to create surfaces with different characteristics, and growing cells on each of those surfaces are extremely time-consuming and limit development of the understanding of these effects. Combinatorial and high-throughput techniques are two methods that provide answers to this challenge. Apart from providing an effective data

acquisition, the large amount of data generated from combinatorial and high-throughput techniques requires equally effective and cost-efficient methods for analysis and evaluation. Data mining and data processing techniques are needed to cope with the large amount of information generated by these techniques [36].

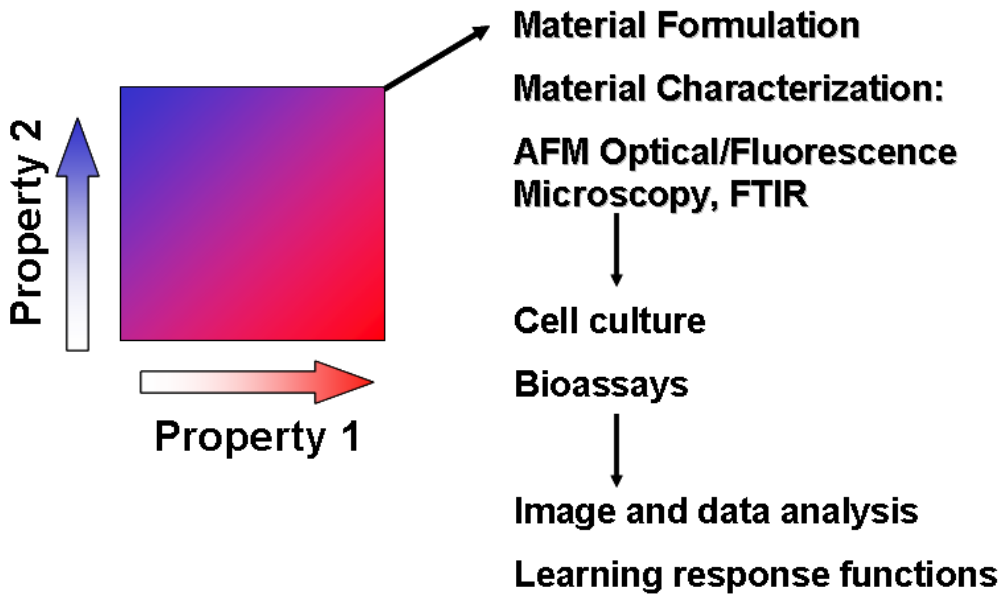

Figure 2. Illustration of Combinatorial Method and its potential applications

Combinatorial techniques have only recently been applied successfully to both chemical and physical aspects of biomaterial design. Chemical synthesis of biodegradable polymers from a diverse set of different monomers has been shown to be successful [2, 3, 37-41, 68]. Briefly, structurally different polymers from combinatorial library of tyrosine-derived polyarylates were synthesized in an array of small 20-ml glass vials. Each vial was charged with the appropriate mixture of monomers and reagents. The monomers were 8 different diacids and 14 different tyrosine-based diphenols. Chemical structure in diacids was used to create structural variations in the polymer backbone, while chemical structure of the diphenols was used to create structural variations at the

polymer pendant chain. From a library of systematically 112 polycarbonates, correlations between structure-property and cellular response were reported as shown in Figure 3.

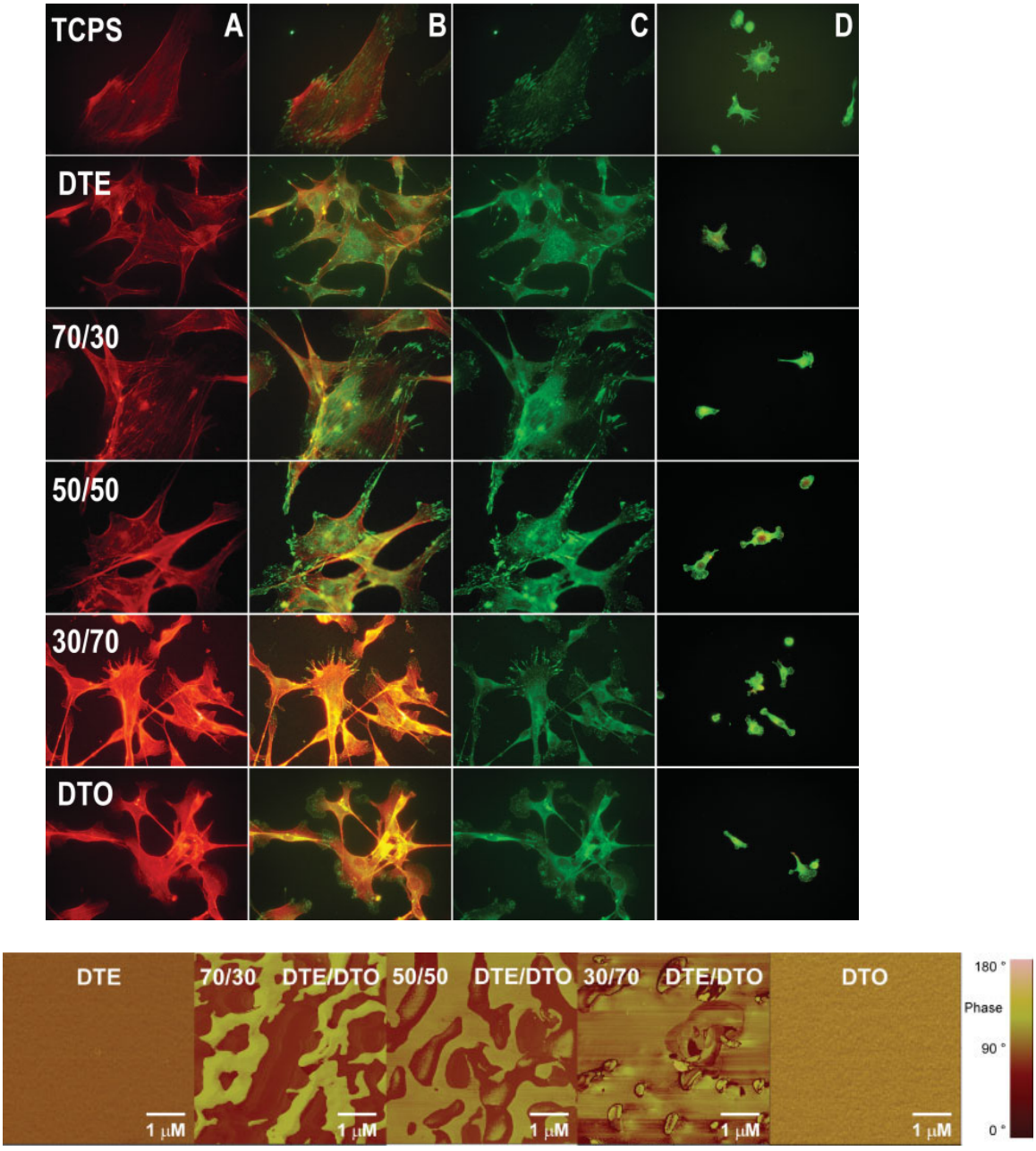

Figure 3. Top: Immunoflurescent staining for actin (A), vinculin (C), overlays of MC3T3 osteoblasts and RAW 264.7. Bottom: Atomic Force Microscopy images of 5 x 5 • m for the respective surfaces used for cell culture [68].

For the physical part, combinatorial methods have shown that phase separation of polymer blends can be utilized to create libraries of varied microstructural physical surface features [1, 42]. Briefly, libraries of biomaterial properties were created combinatorially from composition and annealing temperature gradients. The gradients created diverse arrays of surface properties. It was successfully demonstrated that osteoblast cells cultured directly on those combinatorial surfaces showed different cellular response upon cell-biomaterial interaction as shown in Figure 4. A similar approach is to be followed in this research.

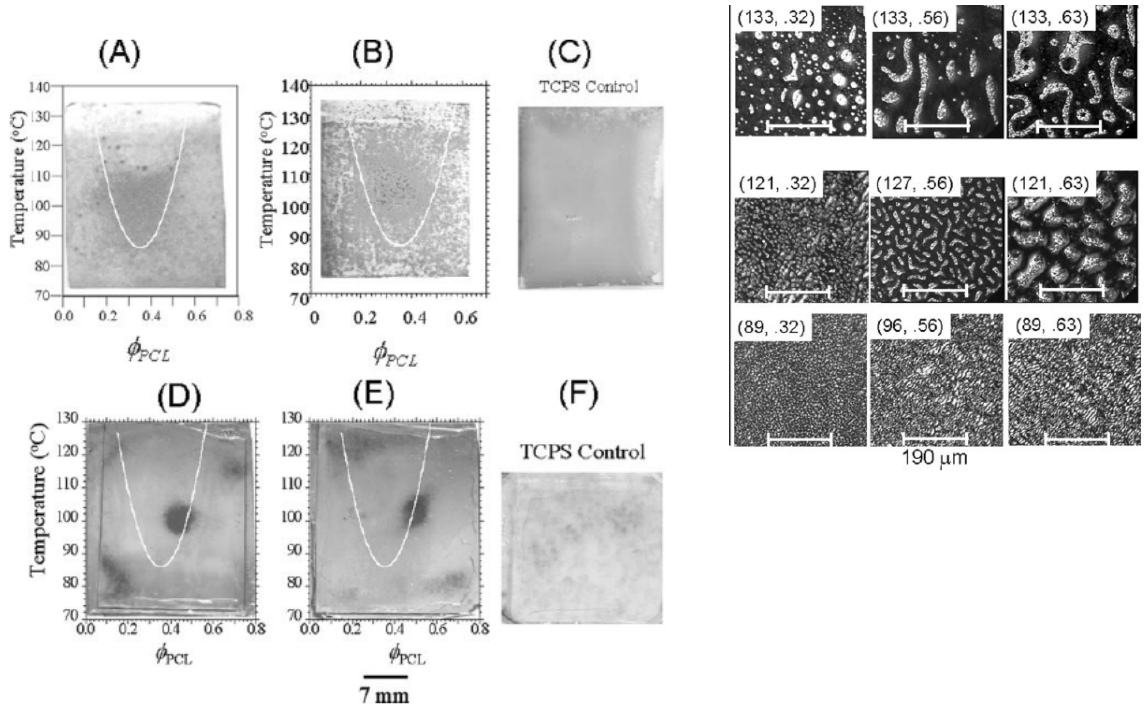

Figure 4. (A) Safranin stained and (B) alkaline phosphatase (AP) stained library after 5-day culture with UMR-106 cells showing preferential adhesion and AP expression on regions approximately within the PDLA/PCL two-phase LCST regime. (D, E) AP stained libraries after 5-day culture with MC3T3-E1 cells. (C, F) AP stained tissue culture polystyrene control slide after 5 days, cultured with UMR-106 and MC3T3-E1 cells, respectively. *Insert:* phase-separated PDLA-PCL blend library visualized with cross-polarized microscopy, scale bar is 190 • m, and the numbers in parentheses were T and % weight of PCL [42].

1.2. Combinatorial Design of Biomaterial

1.2.1. Desired Properties of Biomaterial

An ideally engineered tissue comprising of live cells seeded into a synthetic degradable matrix would have the same mechanical properties as of the natural tissue it is designed to replace. The focus of this research is on osteoblast cells whose natural environment is a multi component ECM. Therefore, the desired biomaterial should resemble ECM in its chemical, mechanical and surface properties. The polymer is chosen taking into account several factors as follows:

a. biocompatibility and degradability
b. ability to be patterned
c. contrast of adhesive and non-adhesive chemistry for cellular adhesion
d. mechanical strength.

The primary surface properties of interest in this research are chemical pattern, microstructure and surface roughness of different domains. Chemical pattern is created by using adhesive and non-adhesive polymer upon cellular attachment. Microstructure is the two dimensional pattern (size and spacing) of adhesive and non-adhesive sub domains. Surface roughness is the three dimensional topographic pattern of the surface and is dependent on microstructure. These will be used to describe surface properties of biomaterial that are related to cellular response.

1.2.2. Choice of materials

Previously, studies with **poly(d,l-lactide) (PDLA)** and **poly(caprolactone) (PCL)** system have been reported [1, 42]. These two biodegradable, biocompatible mates

have a modest difference in hydrophobicity, which leads to some degree of preferential protein andsorption and cell attachment on PDLA. To explore a better hydrophobic versus hydrophilic contrast of the two polymers in the blend, we desire to develop a method for blending and patterning PEG and PCL. Some properties of these polymers are given in Table 1.

Table 1. Physical Properties of the Pure Polymer (data was provided from supplier unless indicated otherwise).

Polymer	**Tg (^{o}C)**	**Tm (^{o}C)**	**Density (g/ml)**	**Water contact angle (^{o})**	**Young's modulus (GPa)**	**Tensile strength (MPa)**
PEG M_w =2,000	-44	49.1	1.104	20-25[43][1]	3.68[43][2]	2.55[43][3]
PCL M_w =80,000	-60	60	1.145	79.2	0.15 [42]	20.1 [42]

Young's modulus is the indicator how stiffness or the amount of force required to elongate, i.e. the material elasticity. Tensile strength indicates the stress (force/area) at which a material can withstand breaking. From the values above, PEG is more flexible than PCL; but it has less material strength compared to PCL. Therefore, PEG and PCL mixtures may be suitable candidates for biomaterials with adjustable mechanical properties.

Both PEG and PCl are biocompatible and biodegradable. PEG is a well-known protein and cell-repellant surface. Increased PEG content in biomaterial has been proven to reduce protein adsorption and cell attachment [6, 38, 39, 44]. Many ECM and serum

[1] Extrapolated value for PEG 2000.
[2] Extrapolated value for PEG 2000, as a function of porosity. Porosity ranges from 5 to 22%
[3] Extrapolated value for PEG 2000.

proteins have been shown to adsorb well on PCL, due to its hydrophobic character, which can potentially enhance cellular attachment on biomaterial surfaces [45, 46].

The drawback of using PEG is that especially at low molecular weight it is highly soluble in aqueous media [47]. Therefore, PEG needs to be crosslinked to slow down the dissolution to a time scale suitable for tissue engineering.

1.2.3. Choice of methods to design biomaterial

1.2.3.1. Creation of patterning and contrast by phase separation

We desire a micropatterning method that can be extended to 3D tissue engineering scaffold. Previous studies have used phase separation of polymer blends induced by heating the film at temperatures within two-phase region [1]. This process is compatible with 2D and 2D scaffold and creates physically distinct sub domains on the surface of the polymer. We aim to use polymers with contrast in cell "adhesiveness", which phase separate to induce microstructure patterns of adhesive and non-adhesive sub domains.

Incompatibility in the chemical structure and molecular weight of the two components leads to phase separation. The use of blends with a library of surface properties resulting from phase separation can be generated within one combinatorial sample. Lower Critical Solution Temperature (LCST) or Upper Solution Temperature (UCST) phase separation induce different surface microstructure for the library as it has been studied previously [1, 42, 48] It is known that PDLA and PCL have an LCST. Here we expect that PEG-PCL with even greater difference chemistry, to phase separate also.

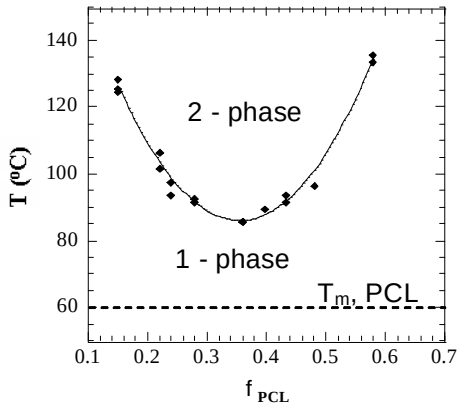

Figure 5. Cloud point curve showing LCST type phase separation in PDLA/PCL system [42]. Cross-polarized microscopy imaging of the phase-separated library was shown in the insert of Figure 4.

There are two degrees of freedom that determine the state of a binary system with two phases. In this study, blend composition and annealing temperature are the variables chosen to control phase separation. Each **composition (•)** and **annealing temperature (T)** will give different degrees of equilibrium phase separation. Elevated temperature for annealing basically moves the condition from 1 phase into 2 phase region (Figure 5). Generally, structures become larger as T moves deeper into 2-phase region and as time proceeds.

The high-throughput creation of surfaces with different characteristics is achieved by phase separation of the polymer blends. Therefore, • , and T become possible control variables to determine the surface characteristics.

1.2.4. Utilizing phase separation in Combinatorial Technique for Biomaterial Design

Phase separation has been shown to be a good means for creating microstructure and surface roughness combinatorial libraries [1,42]. The control variables are • , T, and

film thickness (h). For each sample, two of these variables from • , T, and h can be varied to create two dimensional arrays of data in the surface properties library.

For imaging, crystallinity difference is used to observe the microstructure in an easier way. This is made possible because crystallinity contrast of the two phases can be observed by cross-polarized optical microscopy; the brighter area is the more crystalline phase of the two phases in the phase separated sample. PCL has a unique combination of properties to serve this purpose. Other than its crystalline nature, PCL is also the more hydrophobic part of the blend. Therefore, in PCL-PEG blends, brighter areas under a cross polarized microscope will correspond to the adhesive sub domain.

1.3. Significance

Potential uses of results from this research include cellular biology, tissue engineering, and material science. Fast, cheap and effective surface library design and scanning of properties and cellular response in combinatorial method can be used for biomaterial design for drug-delivery coatings, for example material whose porosity increases as the immersion time in aqueous media is increased; or for characterization and scanning of cellular response to different surface properties in cellular biology studies.

When translated into 3D structure, the significance of bioactive material could reach as far as tissue engineering for ‘difficult-to-grow’ cell lines, such as osteoblast. With proper design to adjust degradation time, 3D scaffold of bioactive material can enhance invasion of osteoblast to re-grow its structure and gain appropriate strength; the scaffold degrade completely when the osteoblast structure is self-sufficient.

1.4. Hypotheses and Specific Aims

The hypotheses are:

1. Phase separation between PCL and modified PEG will create diverse microstructures on the surface which provide patterned size contrast in adhesive versus non-adhesive sub domain, with enhanced deconvolution between physical and chemical properties, as well as between different aspects within the physical properties itself.

2. Surface properties have strong effects to adherent cells' adhesion and spreading.

The specific aims are:

1. **Develop patterned surface libraries with enhanced adhesive/non-adhesive contrast.**

The systems under study will be blends of **poly(ethylene glycol) (PEG)** with biodegradable polymers. The challenge of aim 1 is to develop a reasonably simple approach to incorporating cell non-adhesive PEG into a mechanically-robust and non-water-soluble matrix of a cell adhesive biodegradable polymer. Several crosslinking and copolymerization strategies will be explored.

2. **Screen cell functions against specific surface patterns and features.**

MC3T3-E1 osteoblasts will be cultured on patterned libraries of materials developed in aim 1. A database of cell adhesion and cell spreading response as a function of surface physical and chemical properties will be constructed.

3. **Utilize data mining and statistical approaches to demonstrate knowledge discovery.**

Statistical analysis and knowledge discovery approaches will be applied to the complex database developed in aim 2, to identify the surface properties (or combinations) that have the most significant effects on cell functions.

1.5. References

1. Meredith, J.C., et al., *Combinatorial characterization of cell interactions with polymer surfaces.* J Biomed Mater Res, 2003. **66A**(3): p. 483-90.
2. Brocchini, S., K. James, V. Tangpasuthadol, and J. Kohn, *A combinatorial approach for polymer design.* J. Amer. Chem. Soc., 1997. **119**(19): p. 4553-4554.
3. Brocchini, S., et al., *Structure-property correlations in a combinatorial library of degradable biomaterials.* J Biomed Mater Res, 1998. **42**(1): p. 66-75.
4. B. J. Spargo, e.a., *Spatially controlled adhesion, spreading, and differentiation of endothelial cells on self-assembled molecular monolayer.* Proc. Nat. Acad. Sci, 1994. **91**: p. 11070-11074.
5. C. S. Ranucci, P.V.M., *Polymer Substrate topography actively regulates the multicellular organization and liver-specific functions of cultured hepatocytes.* Tissue Eng., 1999. **5**: p. 407-420.
6. Evangelos Tziampazis, J.K., Prabhas V. Moghe, *PEG-variant biomaterials as selectively adhesive protein templates: model surfaces for controlled cell adhesion and migration.* Biomaterials, 2000. **21**: p. 511-520.
7. Ratner BD, C.D., Horbett TA, Lenk TJ, Lewis KB, Rapoza RJ, *Biomolecular and Surfaces.* Vac. Sci. Technol. A., 1990. **8**(3): p. 2306-2317.
8. Sarikaya, M., et al., *Molecular biomimetics: nanotechnology through biology.* Nat Mater, 2003. **2**(9): p. 577-85.
9. Christopher S. Chen, e.a., *Geometric control of cell life and death.* Science, 1997. **276**(5317): p. 1425-1428.
10. Chen, G., Y. Imanishi, and Y. Ito, *Effect of protein and cell behavior on pattern-grafted thermoresponsive polymer.* J Biomed Mater Res, 1998. **42**(1): p. 38-44.
11. A. Garcia, P.D., D. Boettiger, *The effect of surface reaction stage on fibronectin-mediated adhesion of osteoblast-like cells to bioactive glass.* J. Biomed. Mater. Res., 1998. **40**: p. 48-56.
12. A. Garcia, P.D., D. Boettiger, *Modulation of cell proliferation and differentiation trhough substrate-dependent changes in fibronectin conformation.* Mol. Biol. Cell, 1999. **10**: p. 785-798.
13. Braun, R., M. Sarikaya, and K. Schulten, *Genetically engineered gold-binding polypeptides: structure prediction and molecular dynamics.* J Biomater Sci Polym Ed, 2002. **13**(7): p. 747-57.

14. Bruggemann, O., *Molecularly imprinted materials--receptors more durable than nature can provide.* Adv Biochem Eng Biotechnol, 2002. **76**: p. 127-63.
15. S. Huang, D.I., *Shape-dependent control of cell growth, differentiation, and apoptosis: Switching between attactors in cell regulatory network.* Exp. Cell. Res., 2000. **261**: p. 91-103.
16. D. Itoh, S.Y., S. Kuroda, H. Kondo, A. Umezawa, K. Ohya, . Ohyama, S. Kasugai, *Enhancement of osteogenesis on hydroxyapatite surface coated with synthetic peptide (EEEEEEEPRGDT) in vitro.* 2002: p. 292-297.
17. D.H. Davis, C.S.G., R.W. Johnson, T.A. Desai, *Immobilization of RGD to <111> silicon surfaces for enhanced cell adhesion and proliferation.* Biomaterials, 2002. **23**: p. 4019-4027.
18. Kao, W.J., *Evaluation of protein-modulated macrophage behavior on biomaterials: designing biomimetic materials for cellular engineering.* Biomaterials, 1999. **20**: p. 2213-2221.
19. L. Kam, W.S., J. N. Turner, R. Bizios, *Selective adhesion of astrocytes to surfaces modified with immobilized peptides.* Biomaterials, 2002. **23**: p. 511-515.
20. M. C. Porte-Durrieu, C.L., F. Villars, F. Lefebvre, S. Dutoya, A. Guette, L. Bordenave, C. Baquey, *Development of RGD peptides grafted onto silica surfaces: XPS characterization and human endothelial cell interaction.* 1999: p. 368-375.
21. P. Banerjee, D.J.I., A.M. Mayes, L.G. Griffith, *Polymer latexes for cell-resistant and cell-interactive surfaces.* 2000.
22. S.P. Massia, J.S., *Immobilized RGD peptides on surface-grafted dextran promote biospecific cell attachment.* 2001: p. 390-399.
23. Chen CS, e.a., *Cell Shape provides global control of focal adhesion assembly.* Biochemical and Biophysical Research Communication, 2003. **307**: p. 355-361.
24. John l. Tan, J.T., Dana M. Pirone, Darren S. Gray, Kiran Bhadriraju, Christopher S. Chen, *Cells lying on a bed of microneedles: An approach to isolate mechanical force.* PNAS, 2003. **100**(4): p. 1484-1489.
25. Gray DS, T.J., Chen CS, *Repositioning of cells by mechanotaxis on surfaces with micropatterned Young's modulus.* Journal of Biomedical Material Research, 2003. **66A**: p. 605-614.
26. Y. W. Fan, F.Z.C., L.N.Chen, Y. Zhai, Q.Y. Xu, I-S. Lee, *Adhesion of neural cells on silicon wafer with nano-topographic surface.* Applied Surface Science, 2002. **2002**(187): p. 313-318.
27. Hirokaju Kaji, e.a., *Microelectrochemical Approach to Induce Local Cell Adhesion and Growth on Substrates.* 2004. **20**: p. 16-19.
28. B. D. Boyan, T.W.H., D. D. Dean, Z. Schwartz, *Role of material surfaces in regulating bone and cartilage cell response.* Biomaterials, 1996. **17**: p. 137-146.
29. E. Ostuni, C.S.C., D.E. Ingber, G.M. Whitesides, *Selective Deposition of Proteins and Cells in Arrays of Microwells.* Langmuir, 2001. **17**: p. 2828-2834.
30. Gray, D.S., J. Tien, and C.S. Chen, *Repositioning of cells by mechanotaxis on surfaces with micropatterned Young's modulus.* J Biomed Mater Res, 2003. **66A**(3): p. 605-14.
31. Tan, J.L., et al., *Cells lying on a bed of microneedles: an approach to isolate mechanical force.* Proc Natl Acad Sci U S A, 2003. **100**(4): p. 1484-9.

32. E. Ostuni, R.K., C.S. Chen, D.E. Ingber, G.M. Whitesides, *Patterning Mammalian cells Using Elastomeric Membranes.* Langmuir, 2000. **16**: p. 7811-7819.
33. Wójciak-Stothard B, M.Z., Korohoda W, Curtis A and Wilkinson C, *Activation of macrophage-like cells by multiple grooved substrata:Topographical control of cell behavior.* Cell Biology International, 1995. **19**: p. 485-490.
34. Folkman J, M.A., *Role of cell shape in growth control.* Nature, 1978. **273**: p. 345-349.
35. Chicurel ME , C.S., Ingber DE, *Celular control lies in the balance of forces.* Current Opinion in Cell Biology, 1998. **10**: p. 232-239.
36. Weber, N., et al., *Small changes in the polymer structure influence the adsorption behavior of fibrinogen on polymer surfaces: validation of a new rapid screening technique.* J Biomed Mater Res, 2004. **68A**(3): p. 496-503.
37. Schachter, D.M.a.J.K., *A synthetic polymer matrix for the delayed or pulsatile release of water-soluble peptides.* J. Control. Rel, 2002. **78**: p. 143-153.
38. Yu, C., S.S. Mielewczyk, K.J. Breslauer, and J. Kohn, *Tyrosine-PEG-derived poly(ether carbonate)s as new biomaterials. Part II: Study of inverse temperature transitions.* Biomaterials, 1999. **20**(3): p. 265-272.
39. Yu, C.a.J.K., *Tyrosine-PEG-derived poly(ether carbonate)s as new biomaterials. Part I: Synthesis and Evaluation.* Biomaterials, 1999. **20**(3): p. 253-264.
40. Tangpasuthadol, V., S.M. Pendharkar, and J. Kohn, *Hydrolytic degradation of tyrosine-derived polycarbonates, a class of new biomaterials. Part I: Study of model compounds.* Biomaterials, 2000. **21**: p. 2371-2378.
41. Jack R. Smith, A.S., Norbert Weber, Doyle Knight, Sascha Abramson, Joachim Kohn, *Integration of Combinatorial Synthesis, Rapid Screening, and Computational Modeling in Biomaterial Development.* Macromolecules Rapid Communication, 2004. **25**: p. 127-140.
42. J.C. Meredith, E.J.A., *LCST Phase Separation in Biodegradable Polymer Blends: poly(D,L-lactide) and poly(sigma-caprolactone).* Macromolecules Chemical Physics, 2000. **201**: p. 733-739.
43. Muhammed A. Al-Nasassrah, F.P., J. Michael Newton, *The effect of an increase in chain length on the mechanical properties of polyethylene glycols.* European Journal of Pharmaeutics and Biopharmaeutics, 1998. **46**: p. 31-38.
44. Faucheux, N.S., R.; Lutzow, K.; Werner, C.; Groth, T., *elf-assembled monolayers with different terminating groups as model substrates for cell adhesion studies.* Biomaterials, 2004. **25**(14): p. 2721-2730.
45. Emanuele Ostuni, B.A.G., Milan Mrksich, Carmichael S. Roberts, George M. Whitesides, *Adsorption of Proteins into Hydrophobic Sites on Mixed Self-Assembled Monolayers.* Langmuir, 2003. **19**: p. 1861-1872.
46. Alves, C.M.R., R. L.; Hunt, J. A., *Preliminary study on human protein adsorption and leukocyte adhesion to starch-based biomaterials.* Journal of Materials Science: Materials in Medicine, 2003. **14**(2): p. 157-165.
47. C.M. Nelson, S.R., J.L. Tan, C.S. Chen, *Degradation of Micropatterned Surfaces by Cell-dependent and Independent Processes.* Langmuir, 2003. **19**: p. 1493-1499.

48. Schauer, T.E., Claus D, *Organic polymer treatment - the way to modern pigments.* European Coatings Journal, 2003. **3**: p. 114-120.
49. J. Brandup, E.H.I., and E.A. Grulke; associate editors, A. Abe, D.R. Bloch., *Polymer Handbook.* 1999. **4**.
50. Tadakoro, H., *Structure and properties of crystalline polymers.* Polymer, 1984. **25**(2): p. 147-164.
51. Wenbing Hu, V.B.F.M., *Liquid-liquid demixing in binary polymer blend driven solely by the component-selective crystallizability.* Journal of Chemical Physics, 2003. **119**(20): p. 10953-10957.
52. M. Doytcheva, D.D., R. Stamenova, C. Tsvetanov, *UV-initiated crosslinking of Poly(ethylene oxide) with pentaerythritol Triacrylate in solid state.* Macromolecules Material Engineering, 2001. **286**(1): p. 30-33.
53. Haugland, R.P., *Handbook of Fluorescent Probes and Research Products.* 2002. **9th Edition**: p. 461.
54. Kovacs, A.J.G., A.; Straupe, C.*] Isothermal growth, thickening, and melting of poly(ethylene oxide) single crystals in the bulk.* Journal of Polymer Science, 1974. **50**: p. 283-325.
55. G Natta, I.W.B., G. Allegra, Acc. Naz. Lincei Rend, 1961. **31**: p. 350.
56. D.A. Winesett, S.S., J. Luning, H. Ade, *Tuning substrate surface energies for blends of polystyrene and poly(mthyl methacrylate).* Langmuir, 2003. **19**: p. 8526-8535.
57. Orban, J.M.C., Toby M.; Wagner, William R.; Jankowski, Ron., *Easily grafted polyurethanes with reactive main chain functional groups. Synthesis, characterization, and antithrombogenicity of poly(ethylene glycol)-grafted poly(urethanes).* Journal of Polymer Science, Part A: Polymer Chemistry, 1999. **37**(17): p. 3441-3448.
58. Henn, G.S., M.; Poths, H.; Ruecker, M.; Rabe, J. P., *Influence of order in thin smectic polymer films on the structure at the surface.* Physica B: Condensed Matter (Amsterdam), 1996. **221**(1-4): p. 174-184.
59. Doye, J.P.K., *Computer simulations of the mechanism of thickness selection in polymer crystals.* Polymer, 2000. **41**(25): p. 8857-8867.
60. Chattopadhyay, S.M., J. Carson, *Instability and dewetting of conducting-insulating polymer thin-film bilayers.* Macromolecular Rapid Communications, 2004. **25**(1): p. 275-279.
61. Patel, N., et al., *Printing patterns of biospecifically-adsorbed protein.* J Biomater Sci Polym Ed, 2000. **11**(3): p. 319-31.
62. A. El-Ghannam, L.S., J. Jones, *Laminin-5 coating enhances epithelial cell attachment, spreading, and hesmidesmosome assembly on Ti-6Al-4V implant material in vitro.* J. Biomed. Mater. Res., 1999. **41**: p. 30-40.
63. A. El-Ghannam, P.D., I. M. Shapiro, *effect of serum proteins on osteoblast adhesion to surface-modified bioactive glass and hydroxyapatite.* J. Orthopaed. Res., 1999. **17**: p. 340-345.
64. Aaron S. Goldstein, P.A.D., *Effect of adsorbed fibronectin concentration on cell adhesion and deformation under shear on hydrophobic surfaces.* Journal of Biomedical Material Research, 2002. **59**(4): p. 665-675.
65. Bruce Albert, e.a., *Molecular Biology of the Cell.* 2002. **4th Edition**.

66. Su, Jing; Zapata, Pedro; Meredith, J. Carson, *Knowledge discovery applications in high-throughput polymer characterization,* Materials Research Society Symposium Proceedings, 2006, 894.
67. Su, Jing; Meredith, Carson, *Knowledge discovery applications in combinatorial biomaterial surface design.* PMSE Preprints, 2005. **93**: p 1049.
68. Bailey, LeeAnn, et al. *Cellular Response to Phase-separated Blends of Tyrosine-derived Polycarbonates,* J. Biomed Mat Res A, 2006. **76a**(3): p. 491.
69. Kholodovych, Vladyslav, et al. *Accurate predictions of cellular response using GSPR: a feasibility test of rational design of polymeric biomaterial,* Polymer, 2004. **23**: p 7367-7379.

CHAPTER 2

EXPERIMENTAL METHODS

2.1. Micropatterned Polyurethane Preparation

Poly(ethylene glycol) (**PEG**, M_w=2,000, Sigma-Aldrich), poly(caprolactone) (**PCL** M_w=80,000, M_w/M_n=1.43, Aldrich) solutions were prepared in chloroform ($CHCl_3$, Aldrich). PCL was selected at high molecular mass (M_w =80000) compared to the small PEG (M_w=2000) to reduce the end-to-end crosslinking of PCL-PCL and PCL-PEG. Therefore we expect two phases in the product: a PEG-rich polyurethane phase (that itself contains hard domains of MDI) and a PCL-rich uncrosslinked phase. The PEG/PCL composition-annealing temperature (• /T) two-dimensional libraries were prepared on 22 mm×22 mm silicon chips. Si was first treated with Piranha solutions (30 % hydrogen peroxide / 70 % sulfuric acid) for an hour at 80 ºC, then etched with Buffered Oxide Etchant **(BOE) 1:6**, JT Baker). Annealing temperature (80 to 120°C) and PCL composition (• $_{PCL}$, 0 to 0.3, mass fraction) gradients were generated along orthogonal directions using methods described previously [6, 31]. The PEG was chain-extended with 4,4 Methylene bis-phenyl diisocyanate (**MDI,** Sigma-Aldrich) and **Pluracol®** (a triol, Mw=430, BASF) in Tetrahydrofuran (**THF,** EMD). Driven by crystallization and LCST (lower critical solution temperature) phase separation mechanisms, PEG and PCL phases were separated to form specific surface phase patterns.

2.2. Chemical composition analysis.

FTIR was used to verify the chemical composition of the gradient films by averaging 32 scans and resolution of 4 cm^{-1}. Spectral analysis was done with PEAKFIT software.

For non-crosslinked films, PCL was identified with its distinct carbonyl peak at ~ 1730 cm^{-1}. PEG is identified with the ether peaks at ~ 1100 cm^{-1}. For crosslinked urethanes, urethane linkages are identified with NH group stretching at ~ 3300-3347 cm^{-1}. [1,2]

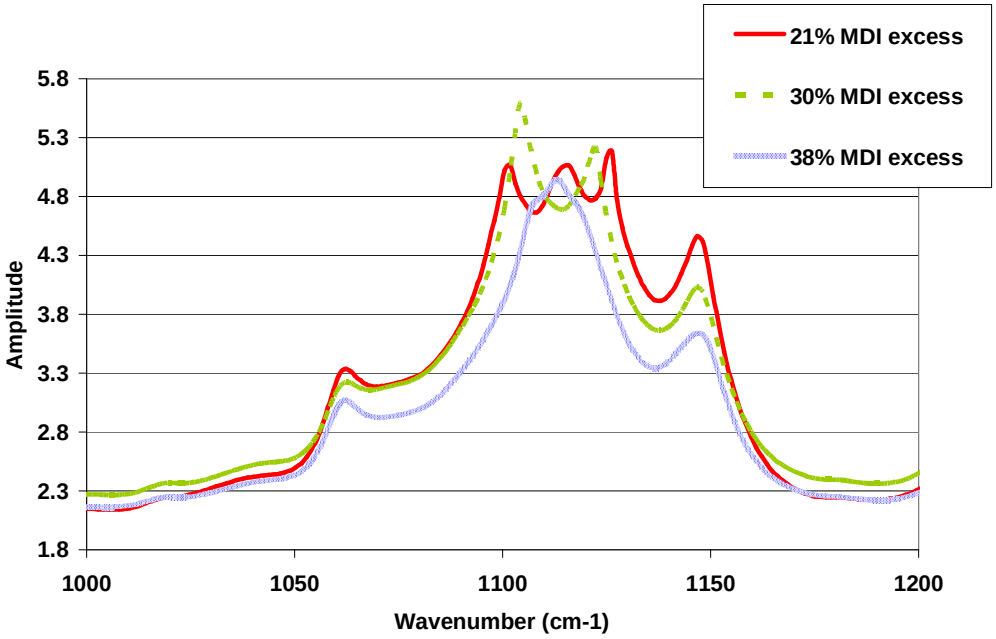

Figure 6. Change in PEG ether groups' ordering after crosslinking with MDI reflected by changes in ether peaks around ~1100 cm^{-1}

2.3. Image Acquisition

Microstructures were studied by crossed-polarized optical microscopy and fluorescent microscopy. These two different types of images were at the same grid of spots on the libraries using a custom, robotic multi-channel microscope. All images and relative information were organized and stored for further image processing and data analysis. Typically, for a 22 mm×22 mm library, at 10× magnification rate, 324 images (1,200 • m×900 • m each) were acquired from distinct locations.

2.4. References

1. Meredith, J.C., Amis, E. J., *LCST Phase Separation in Biodegradable Polymer Blends: poly(D,L-lactide) and poly(sigma-caprolactone).* Macromolecules Chemical Physics, 2000. **201**: p. 733-739.
2. P. Petrini, S.F., A. Piva, M. C. Tanzi, *Design, synthesis and properties of polyurethane hydrogels for tissue engineering.* Journal of Materials Science: Materials in Medicine, 2003. **14**: p. 683-6.

CHAPTER 3

ANALYSIS METHODS

3.1. Image and Data Analysis

Quantitative descriptions of surface lateral patterns and cell proliferation were attained by image processing with ImageJ (NIH) and Matlab™. Dimensionality reduction method via principal component analysis (PCA) was used to handle the complex, correlated dataset. Six descriptors of PCL features were used: area, solidity, eccentricity, major axis length, minor axis length, and PCL-to-PCL spacing. Five descriptors of cell adhesion response were used: cell area, feret diameter, perimeter, eccentricity, and cell density. Because these descriptors are not necessarily independent measures of pattern morphology, PCA [1] was used to reduce the dimensionality of the data. Briefly, the dataset was normalized followed by extraction of eigenvalues and eigenvectors from the singular value decomposition matrix of the normalized dataset. These eigenvalues were used to determine the minimum number of linearly-independent descriptors (eigenvectors) needed to describe at least 99% of the variance in the data.

3.1.1. Principal Component Analysis

The purpose of principal component analysis is to derive a small number of independent linear combinations (principal components) of a set of variables that capture as much of the variability in the original variables as possible.

PCA was introduced by Harold Hoteling [2] in a psychology research application. PCA is a widely used technique to explain correlations within a dataset. It was developed

very extensively in social sciences, where correlations within a dataset were frequently expected. Up to date, this method is still being continuously used and developed [3].

To better illustrate the arrangement of points across many correlated variables, PCA can be used to show the most prominent directions of the high-dimensional data. Using principal component analysis reduces the dimensionality of a set of data. PCA is a way to picture the structure of the data as completely as possible by using as few variables as possible.

For n original variables, n principal components are formed as follows:

- The first principal component is the linear combination of the standardized original variables that has the greatest possible variance.
- Each subsequent principal component is the linear combination of the standardized original variables that has the greatest possible variance and is uncorrelated with all previously defined components.

Each principal component (PC) is calculated by taking a linear combination of an eigenvector of the correlation matrix with a standardized original variable. The eigenvalues show the variance of each component.

PCA is important in visualizing multivariate data by reducing it to dimensionalities that are graphable.

To illustrate, starting with a scatterplot for two highly correlated variables., it is possible to compute a linear combination of the two variables that best captures the

scatter of the points by performing PCA. The results from PCA would be the PCs, in this illustration two PCs were used, with the combination indicated by the P1 line as shown on the left in Figure 7. Rotating and reflecting the plot so that P1 is the variable on the main axis, as seen on the right in Figure 7, gives you the best one-dimensional approximation of a two-dimensional cloud of points. This rotation step will be explained further in the next sections (see Varimax Rotation). The second principal component, P2, describes the remaining variation. This is an example of a principal-component-decomposition for two variables followed by factor rotation. Similarly, the best three-dimensional view of higher dimensional data can be obtained by placing their first three principal components as the spinning axes and examining the plot.

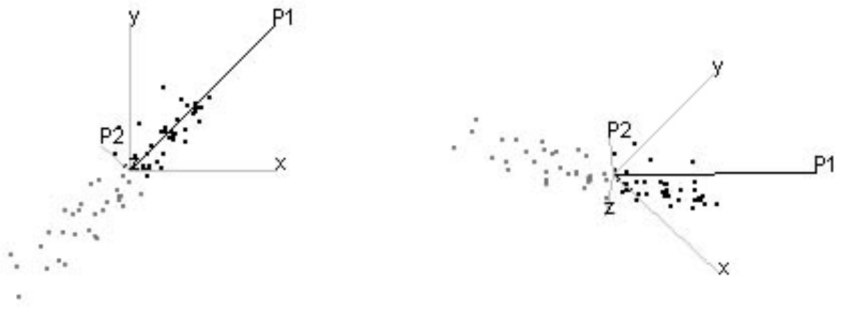

Figure 7. Illustration of two variables before (*left*) and after (*right*) PCA

PCs is shown in columns of values that correspond to the eigenvectors for each of the principal components, in order, from left to right. Using these coefficients to form a linear combination of the original variables produces the principal component variables.

3.1.2. Factor Rotation (Varimax Method)

Rotations are used to better align the directions of the factors with the original variables so that the factors may be more interpretable. Clusters were expected of variables that are highly correlated to define the rotated factors. The rotation's success at clustering the interpretability is highly dependent on the number of factors that were chosen to be rotated.

After the initial extraction, the factors are uncorrelated with each other. If the factors are rotated by an orthogonal transformation, such as varimax, the rotated factors are also uncorrelated. The varimax method tries to make elements of this matrix go toward 1 or 0 to show the clustering of variables.

3.1.3. Clustering

Clustering is the technique of grouping rows together that share similar values across a number of variables. Clustering is an exploratory technique to help understand the clumping structure of a dataset. Three common clustering methods are:

- Hierarchical clustering is appropriate for small tables, up to several thousand rows. It combines rows in an hierarchical sequence portrayed as a tree.
- K-means clustering is appropriate for larger tables, up to hundreds of thousands of rows. It makes a fairly good guess at cluster seed points. It then starts an iteration of alternately assigning points to clusters and recalculating cluster centers. The number of clusters needs to be specified before the start the process. Optimum number of clusters is reached when the reduction of total sum

of distance in the dataset from the nearest clusters slows down (or ‘flatten out’) with respect to addition of cluster center.

- Normal mixtures are appropriate when data is assumed to come from a mixture of multivariate normal distributions that overlap. Maximum likelihood is used to estimate the mixture proportions and the means, standard deviations, and correlations jointly. This approach is particularly good at estimating the total counts in each group. However each point, rather than being classified into one group, is assigned a probability of being in each group. The EM algorithm is used to obtain estimates.

3.1.3.1. K-means clustering

K-means clustering is an iterative follow-the-leader strategy. First, the user must specify the number of clusters, k. Then a search algorithm goes out and finds k points in the data, called seeds, that are not close to each other. Each seed is then treated as a cluster center. The routine goes through the points and assigns each point to the cluster it is closest to. For each cluster, a new cluster center is formed as the means (centroid) of the points currently in the cluster. This process continues as an alternation between assigning points to clusters and recalculating cluster centers until the clusters become stable.

K-means is a doubly-iterative process. The clustering process iterates between two steps in a particular implementation of the EM algorithm:

- The expectation (E) step of mixture clustering assigns each observation a probability of belonging to each cluster.
- For each cluster, a new center is formed using every observation with its probability of membership as a weight. This is the maximization (M) step.

This process continues alternating between the expectation and maximization steps until the clusters become stable.

The k-means approach to clustering performs an iterative alternating fitting process to form the number of specified clusters. The k-means method first selects a set of n points called cluster seeds as a first guess of the means of the clusters. Each observation is assigned to the nearest seed to form a set of temporary clusters. The seeds are then replaced by the cluster means, the points are reassigned, and the process continues until no further changes occur in the clusters. When the clustering process is finished, you see tables showing brief summaries of the clusters. The k-means approach is a special case of a general approach called the EM algorithm, where E stands for Expectation (the cluster means in this case) and the M stands for maximization, which means assigning points to closest clusters in this case.

The k-means method is intended for use with larger data tables, from approximately 200 to 100,000 observations. With smaller data tables, the results can be highly sensitive to the order of the observations in the data table.

Dataset is standardized by Standard Deviation; this means distances are to be calculated so that for each dimension, the difference is scaled by an overall estimate of the standard deviation of each variable.

3.2. Applications of PCA in life sciences

Application of PCA was initially started in a psychology research [2]. However, the current applications of PCA has spread to other fields, including life sciences, especially in the field related to bioinformatics [4-8].

3.3. References

1. Wendy L. Martinez, A.R.M., *Exploratory Data Analysis With Matlab.* 2005: CRC Press.
2. Hoteling, H., *Analysis of a Complex of Statistical Variables with Principal Components*, 1933, Journal of Educational Psychology
3. Heather M. Gray, et al, Science, 2007. **315**: p 619.
4. Aamer, Khaled A., et al *Development of high- throughput combinatorial screening method for probing cell-biomaterials interactions.* PMSE Preprints (2008), 98 838-839.
5. Harris, Nicole, et al. *Rapid discovery of biologically relevant polymer properties: from concept to validation.* PMSE Preprints (2006), 95 1039-1040.
6. Smith, Jack R, et al. *Integration of combinatorial synthesis, rapid screening, and computational modeling in biomaterials development.* Macromolecular Rapid Communications (2004), 25(1), 127-140
7. Treiser Matthew D, et al. *Profiling cell-biomaterial interactions via cell-based fluororeporter imaging.* BioTechniques (2007), 43(3), 361-6, 368.
8. Kohn Joachim, et al. *A new approach to the rationale discovery of polymeric biomaterials.* Biomaterials (2007), 28(29), 4171-7.

CHAPTER 4

DISCOVERY OF UNIQUE MICROPHASE-SEPARATED FEATURES IN POLYURETHANES AND POLYURETHANE-POLYESTER BLENDS

ABSTRACT

Combinatorial methods (CM), employed in parallel with high-throughput screening (HTS), allow efficient exploration of complex materials in multidimensional parameter space. In this study the CM-HTS approach was used to explore microstructures in polyurethanes and polyurethane-polyester blends. In particular, the system studied was a polyurethane based on polyethylene glycol (PEG) blended with linear polycaprolactone (PCL). We identified regions of composition and temperature leading to novel phase-separated microstructures in the 1 to 100 μm range, with minimal degradation (in weight %) in aqueous media. Desired microstructures were observed at triol-to-PEG ratios from 50 to 70 mass %. The microstructures were classified into groups using a density-dependent principle components analysis. Surface features included circular islands, rings, and worms up to 70 μm in size and 1 μm in height, as a function of PCL concentration. The minimum degradation after 1 d immersion in aqueous media was 5.5 mass % at preparation conditions 35% mole excess MDI and 60% by mole Pluracol with respect to the stoichiometric PEG.

4.1. Introduction

One of the most complex challenges facing soft materials science and engineering is the design and development of 'intelligent' biomaterials. These are materials with specific, combined chemical and physical functionalities that interact with cells to create desired biological responses [1-8]. For adhesion-dependent cells, the effect of surface physical features and their coupling with chemistry is significant but remains poorly understood. Surface topography, geometric spacing of chemically-distinct microstructures, and surface mechanical properties are known to influence cellular responses [4, 6, 9-17]. For example, varying the ratio of 'cell adhesive' to 'non-cell adhesive' domain area and spacing imposes a geometric control of fibroblast viability and proliferation [10]. Cell shape and movement (traction and migration) are also affected by substrate modulus [14, 18]. Much of this fundamental research has utilized lithographic techniques to create 2D surfaces with well-controlled spatial and chemical patterns [1, 4, 10, 19-22]. Natural-patterning phenomena based on microphase separation, self-assembly, and crystallization are attractive alternatives for creating three-dimensional structures within the inner surfaces of scaffolds for tissue engineering.. However, the link between cell responses and self-organizing physical surface features of soft, polymeric biomaterials has not been investigated to the same extent as the lithographically-prepared surfaces.

Challenges for phase-separating, microstructured materials characterization include the large number of parameters and the limited ability to predict accurately the microstructures. Combinatorial methods (CM) have recently been applied to characterize soft biomaterial libraries prepared over a large number of compositional and processing

variables. [2, 3, 24-32] High-throughput screening (HTS) provides for rapid measurement of properties on these libraries. Data mining and informatics are utilized to model and analyze the large amount of information generated [23].

For example, discrete libraries of biodegradable polymers synthesized from tyrosine-derived arylate monomers was used along with data mining methods to develop structure-property relationships for fibroblast function [2, 3, 24-28]. Phase separation and dewetting [6, 29-31] of polymer blends can be utilized to create libraries containing continuous gradients of properties including surface energy, crystallinity, composition [32], film thickness (h), and annealing temperature (T). CM methods were used to create biomaterial libraries with composition, thickness and annealing temperature gradients, displaying diverse arrays of surface roughness and lateral microstructure properties. It was successfully demonstrated that cell functions of osteoblasts and aortic smooth muscle cells cultured directly on the libraries showed strong dependence on the extent and type of phase-separation [6, 33, 34]

A generalized understanding of the relationship between surface properties and cellular responses is not yet established for phase-separating biomaterials like PDLA-PCL and PLGA-PCL. This is due in part to the coupling of chemical and physical surface properties inherent to phase-separation in these systems, making it difficult to identify each effect. One potential solution might be the use of a phase-separated biomaterial system with better chemical contrast between domains. Fthis study focuses on developing blends of strongly hydrophilic and hydrophobic materials that have previously been shown to resist or promote cell adhesion, respectively.

CM/HTS methods were applied herein to explore the phase-separated microstructures generated for a family of biomedically-relevant poly(ethylene glycol) (PEG) polyurethanes, and their blends with poly(caprolactone) (PCL), a biodegradable polyester. PEG is chosen because it is biocompatible and resistant to protein and cell adhesion [5, 27, 28, 35]. PCL is chosen based on its excellent cell adhesive properties, biodegradability, and prior history in FDA compliant devices [12, 36]. In addition to biological and chemical aspects, PEG and PCL also have compatible physical and mechanical properties as shown in Table 1. With the advantageous PEG hydrophilicity comes the drawback of PEG's high solubility in water. This problem will be resolved by crosslinking PEG with urethane bonds to reduce its dissolution rate in water. A di-isocyanate and a triol were used to form both di- and trifunctional urethane with the hydroxyl ends of PEG. In addition to providing chemical crosslinks, hydrogen bonds between urethane bonds lead to crystalline hard domains that act as physical crosslinks. These crosslinks, in turn, contribute to the gelation of the crosslinked polymer.

Table 2. Physical Properties of the Pure Polymer (data was provided from supplier unless indicated otherwise)

Polymer	**Tg (^{o}C)**	**Tm (^{o}C)**	**Density (g/ml)**	**Water contact angle (^{o})**	**Young's modulus (GPa)**	**Tensile strength (MPa)**
PEG M_w =2,000	-44	49.1	1.104	20-25[37]	3.68[37]	2.55[37]
PCL M_w =80,000	-60	60	1.145	79.2	0.15[31]	20.1[31]

4.2. Materials and Methods

Micropatterned Polyurethane Preparation. Poly(ethylene glycol) (**PEG**, M_w=2,000, Sigma-Aldrich), poly(caprolactone) (**PCL** M_w=80,000, M_w/M_n=1.43, Aldrich) solutions were prepared in chloroform ($CHCl_3$, Aldrich). PCL was selected at high molecular mass (M_w =80000) compared to the small PEG (M_w=2000) to reduce the end-to-end crosslinking of PCL-PCL and PCL-PEG. Therefore we expect two phases in the product: a PEG-rich polyurethane phase (that itself contains hard domains of MDI) and a PCL-rich uncrosslinked phase. The PEG/PCL composition-annealing temperature (• /T) two-dimensional libraries were prepared on 22 mm×22 mm silicon chips. Si was first treated with Piranha solutions (30 % hydrogen peroxide / 70 % sulfuric acid) for an hour at 80 ºC, then etched with Buffered Oxide Etchant **(BOE) 1:6**, JT Baker). Annealing temperature (80 to 120°C) and PCL composition (• $_{PCL}$, 0 to 0.3, mass fraction) gradients were generated along orthogonal directions using methods described previously [6, 31]. The PEG was chain-extended with 4,4 Methylene bis-phenyl diisocyanate (**MDI,** Sigma-Aldrich) and **Pluracol®** (a triol, Mw=430, BASF) in Tetrahydrofuran (**THF,** EMD). Driven by crystallization and LCST (lower critical solution temperature) phase separation mechanisms, PEG and PCL phases were separated to form specific surface phase patterns.

Chemical composition analysis. FTIR was used to verify the chemical composition of the gradient films by averaging 32 scans and resolution of 4 cm^{-1}. For non-crosslinked films, PCL was identified with its distinct carbonyl peak at ~ 1730 cm^{-1},

while PEG is identified with the ether peak at ~ 1100 cm^{-1}. For crosslinked urethanes, urethane linkages are identified with NH group stretching at ~ 3300-3347 cm^{-1}. [38, 39]

Cell Lines. Osteoblasts were chosen as the mammalian cell line used for for this research. The reasons behind this choice are two-fold. From cellular biology, much research has on this cell line has made this a well-characterized system. For future applications of biomaterials, osteoblast growth and behavior is crucial to a wide range of orthopedic therapies. Such as coating on prosthesis or post-surgery implant to enhance adhesion and healing.

Image Acquisition. Microstructures were studied by crossed-polarized optical microscopy and fluorescent microscopy. These two different types of images were at the same grid of spots on the libraries using a custom, robotic multi-channel microscope. All images and relative information were organized and stored for further image processing and data analysis. Typically, for a 22 mm×22 mm library, at 10× magnification rate, 324 images (1,200 • m×1000 • m each) were acquired from distinct locations.

Analysis. Quantitative descriptions of surface lateral patterns and cell proliferation were attained by image processing with ImageJ (NIH) and Matlab™. Six descriptors of PCL features were used: area, solidity, eccentricity, major axis length, minor axis length, and PCL-to-PCL spacing. Because these descriptors are not necessarily independent measures of pattern morphology, principal component analysis (PCA) [40] was used to reduce the dimensionality of the data. Briefly, the dataset was normalized followed by extraction of eigenvalues and eigenvectors from the singular value decomposition matrix of the normalized dataset. These eigenvalues were used to

determine the minimum number of linearly-independent descriptors (eigenvectors) needed to describe at least 99% of the variance in the data.

4.3. Results and Discussion

The challenge with PEG dissolution in aqueous media was approached by crosslinking it with MDI to create a polyurethane network. The ratio of MDI to PEG was adjusted to find a composition yielding a minimum dissolution after 1 d immersion in aqueous culture media.. The results, shown in Figure 8, indicate an optimal composition at 32 % mole excess of MDI to PEG.

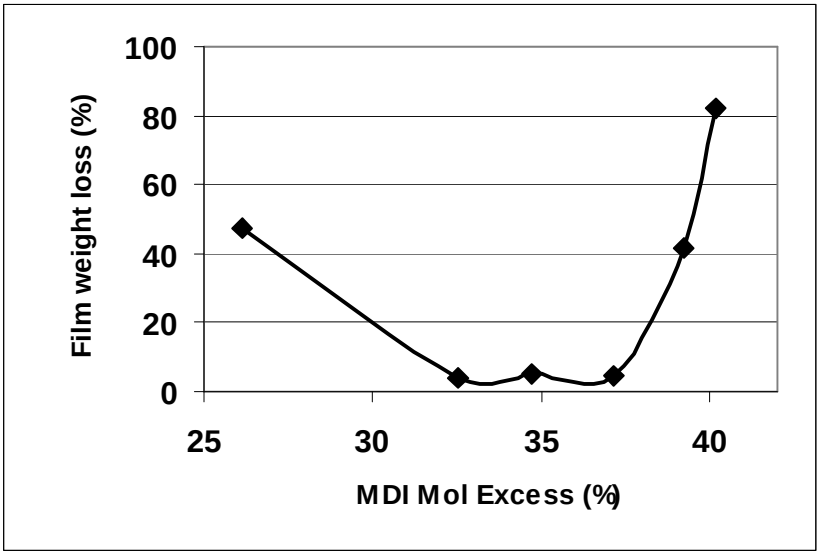

Figure 8. Film weight loss (%) in aqueous media versus Excess MDI with respect to PEG (%)

In addition to MDI, Pluracol™ is used to add some degree of tri-functional crosslinking to PEG to control its dissolution. . Dissolution rate for 3 days immersion

period in aqueous culture media was 5.5 +/- 3.8 %. Mass for Pluracol concentration from 20 % to 80 % relative to the moles of PEG.

Figure 9 illustrates the simultaneous effect of varying Pluracol concentration in addition to adjusting curing temperature. The difference in brightness of the phases shown in Figure 9 was due to differences in birefringence of the phases under cross-polarized light. The PCL-rich phase is more crystalline, hence it shows as the brighter phase compared to the more amorphous, crosslinked PEG-rich phase. Temperature, together with Pluracol concentration, affects the degree of crystallinity of the PEG-rich phase. Increasing annealing temperature at low Pluracol concentration enables the PEG-rich phase structure to have higher birefringence due to its higher crystallinity. However, at high Pluracol concentration, crystallization in the PEG-rich phase is likely more constrained due to the crosslinking, and increasing annealing temperature no longer leads to observable differences in the PEG-rich phase's birefringence under cross-polarized light. Higher annealing temperature enables greater mobility and coalescence of the PCL-rich phase. Hence, at high Pluracol concentration, larger PCL-rich features are shown at higher annealing temperature. High-throughput screening of the library shown in Figure 9 narrows down the region of interest to between 40 % to 70 % Pluracol to PEG mole ratio. This range captures enhanced physical contrast between crystalline and non-crystalline domains under cross-polarized light. This range will be further explored in this study.

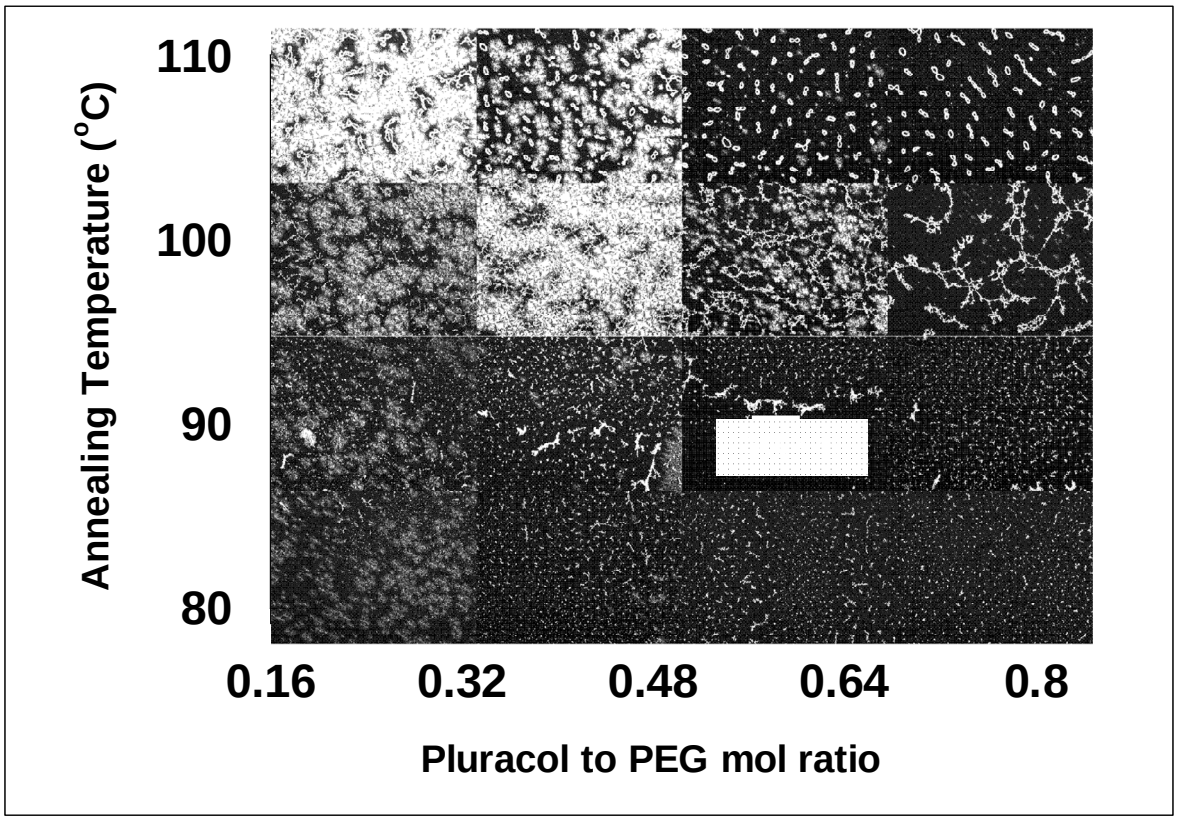

Figure 9. Combinatorial library of phase-separated features at different annealing temperature and Pluracol composition (10x magnification of cross-polarized image).

To cover a wider range of PCL features' size and shape than the ribbon-like features in the region of interest from Figure 9 above, PCL concentration was varied from 0.16 to 0.68 mole ratio of PCL to PEG while maintaining the annealing temperature gradient from 80 to 110°C. Optical cross-polarized micrographs of the library exploring PCL composition (at constant MDI composition at 20% mole excess and Pluracol at 50% mole ratio, both calculated with respect to PEG) is shown in Figure 10. The combinatorial library of surface lateral patterns covers the range of diverse shapes and sizes of the lateral patterns; from several microns circular islands to ~70 um ribbon patterns. The height of the features ranges from 0 to ~ 1 um. Similar d microstructure

have been previously reported to be generated by a flow-induced effect during phase-separation [41, 42]. However, the microstructure reported were at least one-order-of-magnitude smaller than ones reported here.

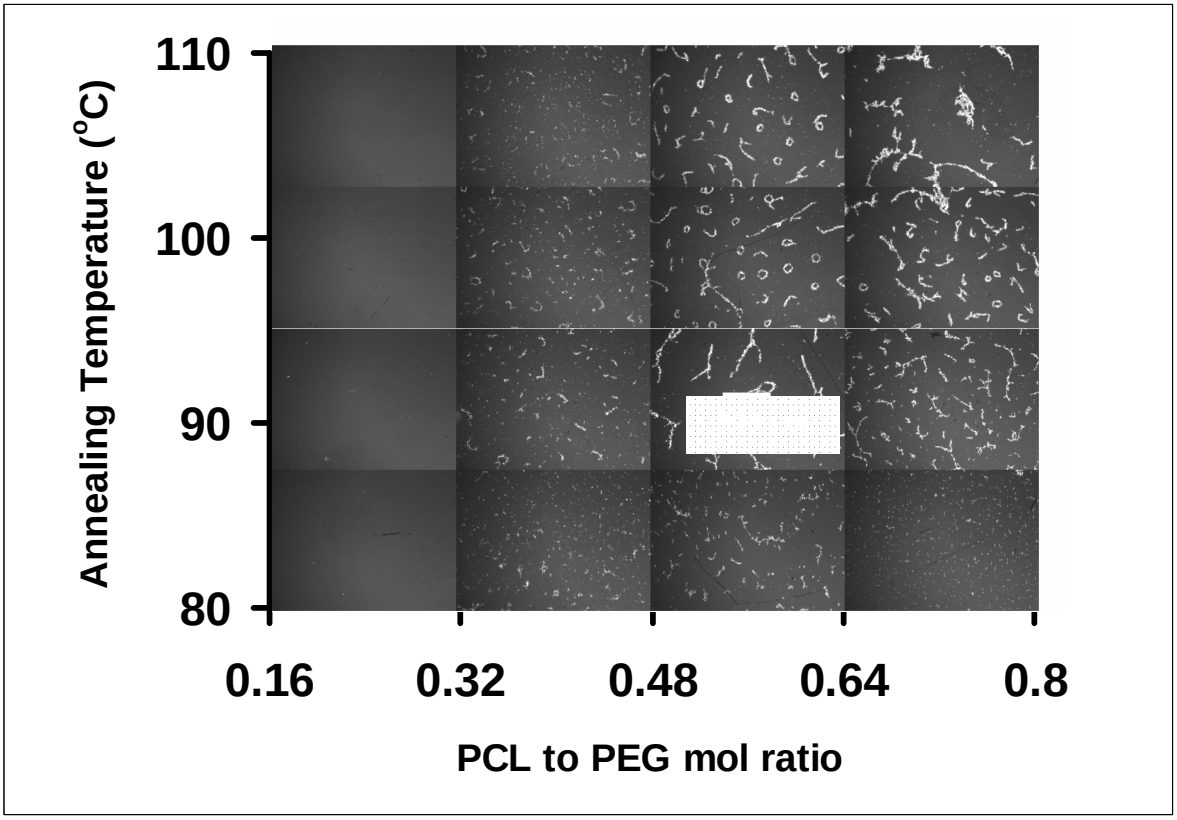

Figure 10. Combinatorial library of phase-separated features at different annealing temperature and PCL composition (10x magnification of cross-polarized image)

Principal component analysis was used to analyze the quantitative data from image analysis of the patterned surfaces represented in Figure 10. Six parameters were be examined: area, solidity, eccentricity, major diameter, minor diameter, and spacing. Spacing is defined as Euclidean distance between the center of mass of one feature to its closest neighbor. Definitions of the other parameters are explained in Table 3. Briefly, the dataset was normalized followed by extraction of eigenvalues and eigenvectors from the

singular value decomposition matrix of the normalized dataset. These eigenvalues were used to determine the minimum number of linearly-independent descriptors (eigenvectors) needed to describe the variance in the data.

Table 3. Definitions of Solidity, Eccentricity, Major Diameter, and Minor Diameter

Parameter	Definition	Illustration
Solidity	Solidity = Solid-fill area/Total area * 100%	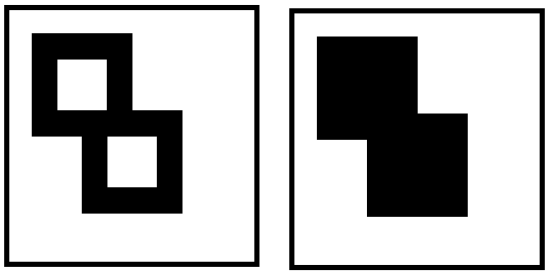 Solidity= 73.3% Solidity=100%
Eccentricity (•)	$e = \sqrt{1 - \frac{b^2}{a^2}}$	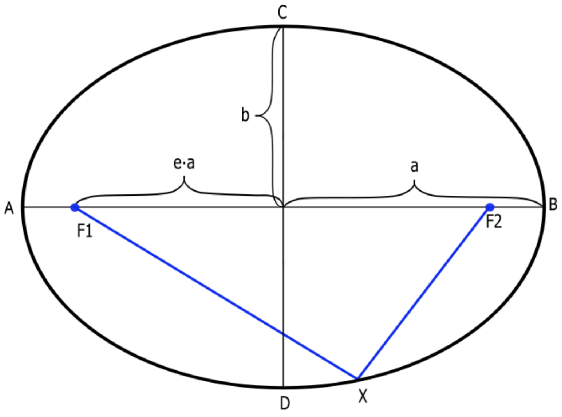
Major Diameter	Length of line AB	
Minor Diameter	Lengh of line CD	

Table 4. Table of Eigen Values for each Principal Component

PC	Eigen Values	Relative Importance of Eigen Values (%)
PC 1	6.39E-02	**51.17**
PC 2	4.32E-02	**34.56**
PC 3	1.63E-02	**13.02**
PC 4	1.37E-03	1.10
PC 5	1.33E-04	0.11
PC 6	5.75E-05	0.05

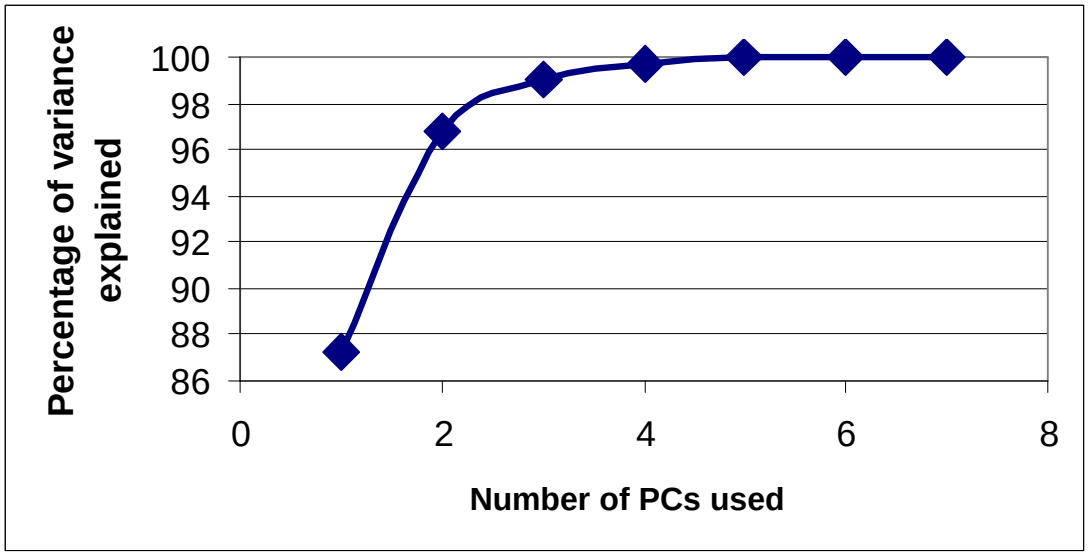

Figure 11. Cumulative percentage of variance explained plotted against the number of PCs used

From Table 4 and Figure 11, the first three PCs captured more than 99% of the variance in the dataset. Furthermore, the principal parameters are identified by the magnitude of the eigenvectors as shown in Table 5. Solidity, eccentricity, and spacing are the principal descriptors in explaining the whole dataset's variance.

Table 5. Eigen Vectors of the dataset extracted with PCA

Factors	**Eig PC 1**	**Eig PC 2**	**Eig PC 3**	**Eig PC 4**	**Eig PC 5**	**Eig PC 6**
Area	-1.78E-04	4.77E-03	-1.58E-02	3.15E-01	-2.49E-01	9.16E-01
Solidity	3.55E-03	**-2.82E-01**	**9.51E-01**	1.25E-01	1.89E-02	-2.01E-02
Eccentricity	-1.08E-02	**9.59E-01**	**2.84E-01**	4.19E-03	1.37E-02	2.18E-03
Major D	-3.10E-04	2.96E-02	-7.80E-02	6.85E-01	-6.03E-01	-4.01E-01
Minor D	6.78E-04	1.48E-02	-9.60E-02	6.45E-01	7.58E-01	-1.75E-02
Spacing	**-1.00E+00**	-1.13E-02	2.77E-04	5.68E-04	6.64E-04	-1.46E-04

One limitation in this conclusion is the correlations that exist between area, solidity, and eccentricity as shown in Figure 12 and Table 7. Solidity and eccentricity exhibit the strongest correlation.. This is due to the dominant shapes inherent in the library. For example, for elongated features (chains) with high eccentricity, the solidity is lower (with 'holes' in the 'chains'). The value of the three principal parameters that characterizes the major shapes observed in the library is shown in Table 6. Analysis was performed on 1000 features visually categorized as chains, worms, or rings, and data was presented as the average values for each shape.

Table 6. Analysis on major shapes in the library (*Bar: 5 • m*)

Shape	Area	Solidity	Eccentricity	Illustration
Chains	41060	0.56	0.84	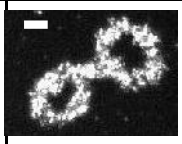
Worms	37700	0.83	0.65	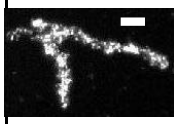
Rings	9250	0.70	0.43	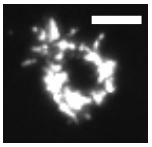

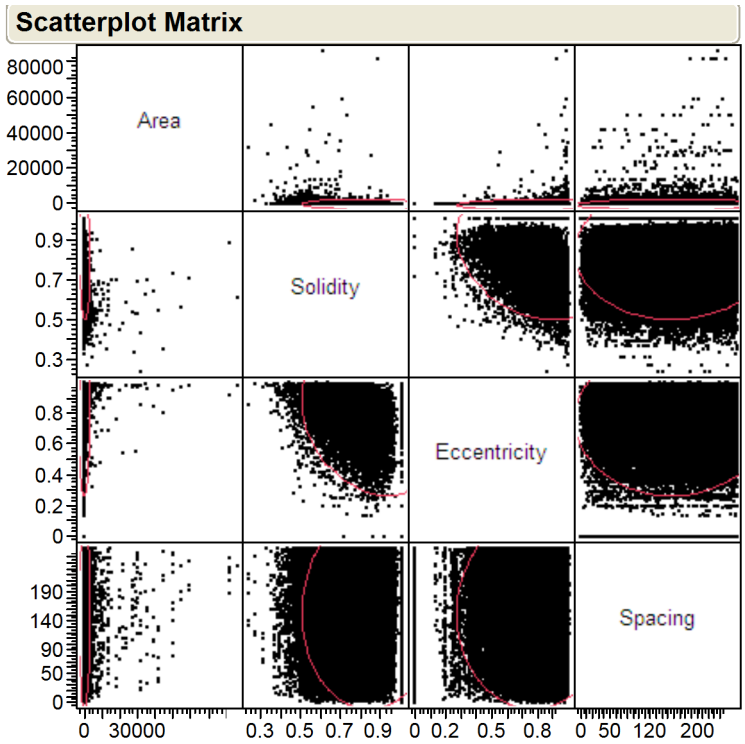

Figure 12. Plot pairwise correlation matrix

Table 7. Pairwise Correlation Table

Multivariate

Correlations

	Area	Solidity	Eccentricity	Spacing
Area	1.0000	-0.1320	0.0443	0.0026
Solidity	-0.1320	1.0000	-0.2672	-0.0025
Eccentricity	0.0443	-0.2672	1.0000	0.0043
Spacing	0.0026	-0.0025	0.0043	1.0000

Inverse Corr

	Area	Solidity	Eccentricity	Spacing
Area	1.0178	0.1317	-0.0099	-0.0023
Solidity	0.1317	1.0939	0.2865	0.0011
Eccentricity	-0.0099	0.2865	1.0770	-0.0039
Spacing	-0.0023	0.0011	-0.0039	1.0000

Partial Corr

	Area	Solidity	Eccentricity	Spacing
Area	.	-0.1248	0.0094	0.0022
Solidity	-0.1248	.	-0.2639	-0.0011
Eccentricity	0.0094	-0.2639	.	0.0038
Spacing	0.0022	-0.0011	0.0038	.

partialed with respect to all other variables

Circular rings and island features dominate over ribbon and worm-like features by the number of occurrences. However, there is no difference in the spatial distribution between circular and elongated shapes. This deconvolution of spatial distribution and shape will likely be a crucial key element in studying cellular response to biomaterials prepared with this blend system.

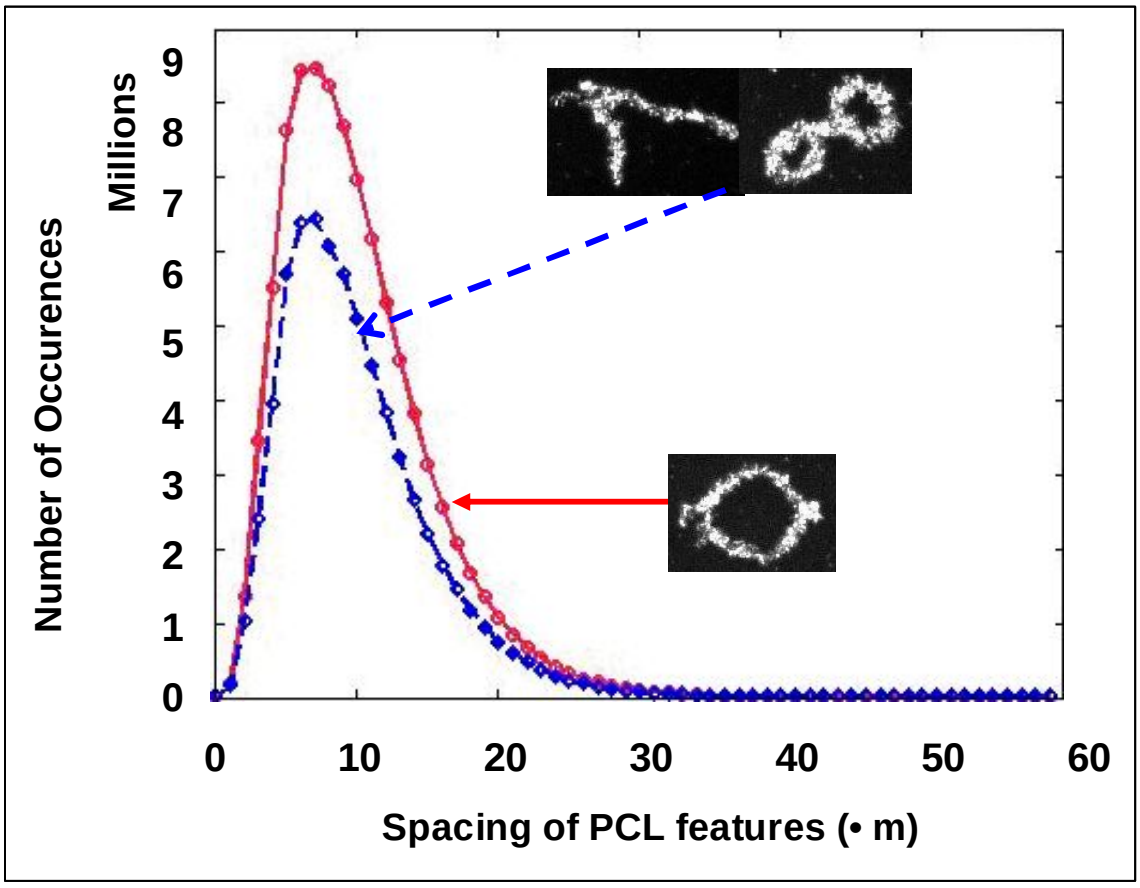

Figure 13. Spacing of PCL features based on different shapes (Red: eccentricity between 0 – 0.75. Blue: eccentricity larger than 0.75)

4.4. Conclusions and Future Directions

PCL-rich features exhibiting a variety of shapes, sizes, and spacings within a PEG-rich phase background was obtained from high-throughput screening of combinatorial libraries in material composition and processing temperature. PCL-rich phase shapes observed included 'rings', 'chains', and 'worms'. Deconvolution of the control of spacing, size, and shape of PCL features was achieved by varying the composition of MDI, the tri-functional chain extender Pluracol, the PCL content, and the annealing temperature. Optimum composition and annealing temperature to achieve minimum weight loss upon immersion into aqueous solution (~ 1 d), and desired visual contrast between surface patterns and background, are achieved at 34% MDI mole excess with respect to PEG, between 40-70% mole ratio of Pluracol to PEG, and at annealing temperature of ~ 110^{o} C. The ability to generate the library with different ratio of adhesive-vs-non-adhesive area within the surface pattern, as well as the effect of shape, orientation, area, and spacing will play an important role for further cellular response studies focusing on effect of surface physical cues on adherent cells.

4.5. References

1. B. J. Spargo, e.a., *Spatially controlled adhesion, spreading, and differentiation of endothelial cells on self-assembled molecular monolayer.* Proc. Nat. Acad. Sci, 1994. **91**: p. 11070-11074.
2. Brocchini, S., K. James, V. Tangpasuthadol, and J. Kohn, *A combinatorial approach for polymer design.* J. Amer. Chem. Soc., 1997. **119**(19): p. 4553-4554.
3. Brocchini, S., et al., *Structure-property correlations in a combinatorial library of degradable biomaterials.* J Biomed Mater Res, 1998. **42**(1): p. 66-75.
4. C. S. Ranucci, P.V.M., *Polymer Substrate topography actively regulates the multicellular organization and liver-specific functions of cultured hepatocytes.* Tissue Eng., 1999. **5**: p. 407-420.

5. Evangelos Tziampazis, J.K., Prabhas V. Moghe, *PEG-variant biomaterials as selectively adhesive protein templates: model surfaces for controlled cell adhesion and migration.* Biomaterials, 2000. **21**: p. 511-520.
6. Meredith, J.C., et al., *Combinatorial characterization of cell interactions with polymer surfaces.* J Biomed Mater Res, 2003. **66A**(3): p. 483-90.
7. Ratner BD, C.D., Horbett TA, Lenk TJ, Lewis KB, Rapoza RJ, *Biomolecular and Surfaces.* Vac. Sci. Technol. A., 1990. **8**(3): p. 2306-2317.
8. Sarikaya, M., et al., *Molecular biomimetics: nanotechnology through biology.* Nat Mater, 2003. **2**(9): p. 577-85.
9. Boyan, B.D., et al, *Role of material surfaces in regulating bone and cartilage cell response.* Biomaterials, 1996. **17**: p. 137-146.
10. Chen, C.S., et al., *Geometric control of cell life and death.* Science, 1997. **276**(5317): p. 1425-1428.
11. E. Ostuni, R.K., C.S. Chen, D.E. Ingber, G.M. Whitesides, *Patterning Mammalian cells Using Elastomeric Membranes.* Langmuir, 2000. **100**(4): p. 1484-9.
12. Emanuele Ostuni, B.A.G., Milan Mrksich, Carmichael S. Roberts, George M. Whitesides, *Adsorption of Proteins into Hydrophobic Sites on Mixed Self-Assembled Monolayers.* Langmuir, 2003. **19**: p. 1861-1872.
13. Fan, Y.W., et al, *Adhesion of neural cells on silicon wafer with nano-topographic surface.* Applied Surface Science, 2002. **187**: p. 313-318.
14. Gray DS, T.J., Chen CS, *Repositioning of cells by mechanotaxis on surfaces with micropatterned Young's modulus.* Journal of Biomedical Material Research, 2003. **66A**: p. 605-614.
15. Hirokaju Kaji, e.a., *Microelectrochemical Approach to Induce Local Cell Adhesion and Growth on Substrates.* 2004. **20**: p. 16-19.
16. Huang, S., Ingber, D., *Shape-dependent control of cell growth, differentiation, and apoptosis: Switching between attactors in cell regulatory network.* Exp. Cell. Res., 2000. **261**: p. 91-103.
17. Tan JL, e.a., *Cells lying on a bed of microneedles: an approach to isolate mechanical force.* PNAS, 2003. **100**(4): p. 1484-9.
18. John I. Tan, J.T., Dana M. Pirone, Darren S. Gray, Kiran Bhadriraju, Christopher S. Chen, *Cells lying on a bed of microneedles: An approach to isolate mechanical force.* PNAS, 2003. **100**(4): p. 1484-1489.
19. Chen CS, e.a., *Cell Shape provides global control of focal adhesion assembly.* Biochemical and Biophysical Research Communication, 2003. **307**: p. 355-361.
20. Folkman J, M.A., *Role of cell shape in growth control.* Nature, 1978. **273**: p. 345-349.
21. Garcia, A., Ducheyne, P., Boettiger, D., *The effect of surface reaction stage on fibronectin-mediated adhesion of osteoblast-like cells to bioactive glass.* J. Biomed. Mater. Res., 1998. **40**: p. 48-56.
22. Garcia, A., Ducheyne, P., Boettiger, D., *Modulation of cell proliferation and differentiation trhough substrate-dependent changes in fibronectin conformation.* Mole. Biol. Cell, 1999. **10**: p. 785-798.

23. Weber, N., et al., *Small changes in the polymer structure influence the adsorption behavior of fibrinogen on polymer surfaces: validation of a new rapid screening technique.* J Biomed Mater Res, 2004. **68A**(3): p. 496-503.
24. Jack R. Smith, A.S., Norbert Weber, Doyle Knight, Sascha Abramson, Joachim Kohn, *Integration of Combinatorial Synthesis, Rapid Screening, and Computational Modeling in Biomaterial Development.* Macromolecules Rapid Communication, 2004. **25**: p. 127-140.
25. Schachter, D.M.a.J.K., *A synthetic polymer matrix for the delayed or pulsatile release of water-soluble peptides.* J. Control. Rel, 2002. **78**: p. 143-153.
26. Tangpasuthadol, V., S.M. Pendharkar, and J. Kohn, *Hydrolytic degradation of tyrosine-derived polycarbonates, a class of new biomaterials. Part I: Study of model compounds.* Biomaterials, 2000. **21**: p. 2371-2378.
27. Yu, C., S.S. Mielewczyk, K.J. Breslauer, and J. Kohn, *Tyrosine-PEG-derived poly(ether carbonate)s as new biomaterials. Part II: Study of inverse temperature transitions.* Biomaterials, 1999. **20**(3): p. 265-272.
28. Yu, C.a.J.K., *Tyrosine-PEG-derived poly(ether carbonate)s as new biomaterials. Part I: Synthesis and Evaluation.* Biomaterials, 1999. **20**(3): p. 253-264.
29. Chattopadhyay, S.M., J. Carson, *Instability and dewetting of conducting-insulating polymer thin-film bilayers.* Macromolecular Rapid Communications, 2004. **25**(1): p. 275-279.
30. Doye, J.P.K., *Computer simulations of the mechanism of thickness selection in polymer crystals.* Polymer, 2000. **41**(25): p. 8857-8867.
31. Meredith, J.C., Amis, E. J., *LCST Phase Separation in Biodegradable Polymer Blends: poly(D,L-lactide) and poly(sigma-caprolactone).* Macromolecules Chemical Physics, 2000. **201**: p. 733-739.
32. P. Petrini, S.F., A. Piva, M. C. Tanzi, *Design, synthesis and properties of polyurethane hydrogels for tissue engineering.* Journal of Materials Science: Materials in Medicine, 2003. **14**: p. 683-6.
33. Hak-Joon Sung, C.M., Chad Johnson and Zorina S. Galis, *The effect of scaffold degradation rate on three-dimensional cell growth and angiogenesis.* Biomaterials, 2004. **25**(26): p. 5735-42.
34. Pedro Zapata, J.S., Andrés J. García, and J. Carson Meredith, *Quantitative High-Throughput Screening of Osteoblast Attachment, Spreading, and Proliferation on Demixed Polymer Blend Micropatterns.* Biomacromolecules, 2007. **8**(6): p. 1907 -1917.
35. Faucheux, N.S., R.; Lutzow, K.; Werner, C.; Groth, T., *Self-assembled monolayers with different terminating groups as model substrates for cell adhesion studies.* Biomaterials, 2004. **25**(14): p. 2721-2730.
36. Alves, C.M.R., R. L.; Hunt, J. A., *Preliminary study on human protein adsorption and leukocyte adhesion to starch-based biomaterials.* Journal of Materials Science: Materials in Medicine, 2003. **14**(2): p. 157-165.
37. Muhammed A. Al-Nasassrah, F.P., J. Michael Newton, *The effect of an increase in chain length on the mechanical properties of polyethylene glycols.* European Journal of Pharmaeutics and Biopharmaeutics, 1998. **46**: p. 31-8.

38. Skarja, G.A., Woodhouse, K.A., *Structure-property relationships of degradable polyurethane elastomers containing an amino acid-based chain extender.* Journal of Applied Polymer Science, 2000. **75**(12): p. 1522-34.
39. Subrata Mondal, J.H., *Structural characterization and mass transfer properties of polyurethane block copolymer: influence of mixed soft segment block and crystal melting temperature.* Polymer International, 2006. **55**: p. 1013-1020.
40. Wendy L. Martinez, A.R.M., *Exploratory Data Analysis With Matlab.* 2005: CRC Press.
41. Gisela Richardson, B.B., Maud Langton, Mats Stading and Anne-Marie Hermansson, *The function of • -crystalline emulsifiers on expanding foam surfaces.* 2004. **18**(4): p. 655-663.
42. Yadong Yin, Y.L., Byron Gates, and Younan Xia, *Template-Assisted Self-Assembly: A Practical Route to Complex Aggregates of Monodispersed Colloids with Well-Defined Sizes, Shapes, and Structures.* J Am Chem Soc, 2001. **123**: p. 8714-8729.

CHAPTER 5

DISCOVERY OF CELLULAR RESPONSES IN ADHESION OF OSTEOBLAST ON PHYSICAL PATTERNS OF BIOMATERIAL'S SURFACE

ABSTRACT

This study demonstrates the efficient screening and exploration of a complex dataset that was generated by high-throughput cell culture on polyurethane libraries. Correlation is observed between surface pattern descriptors and the subsequent cellular adhesion responses described by cellular spreading area, shape, and density. Specific values of spacing in surface patterns are favored for cell adhesion: cells shows preference to adhere close to or on surface patterns composed of polycaprolactone dispersed in a poly(ethylene glycol)-based polyurethane matrix. Furthermore, pattern shapes are correlated with cell spreading behavior: high solidity patterns favor small, circular cells, while low solidity patterns favor large, elongated cells. However, there is no apparent correlation between eccentricity and cell spreading.

5.1. Introduction

The role of surface features in biomaterial design is significant, but poorly understood. The use of micro-patterned surfaces created with microlithography to culture mammalian cells has contributed significantly to studying fundamental cellular biology,

tissue engineering, and cell-based bioelectronics. Spatial control of cellular adhesion and growth is critically important in these fields [1, 2, 3, 4].

It is already known that surface roughness, geometric spacing of adhesive and non-adhesive area, and surface mechanical properties can influence some cellular responses upon adhesion [1, 2, 5, 6]. Cell behavior and cell fate dependence on cellular shape and anchorage in fibroblast cells have been studied for more than two decades [1, 2, 3, 4, 5, 6]. The ratio of adhesive to non- adhesive area, their spacing, and dimensions have been shown to be geometric controls of cellular life and death [2]. It has been reported that cellular shape and movement (traction and migration) are affected by a biomaterial scaffold's mechanical strength, a result crucial to designing successful biomaterials for wound healing [6]. Much of this research has been done with surface patterning techniques adopted from microelectronics used to create model surfaces with well-controlled properties [6]. However, the physical microstructure and topography of applied biomaterials have not been explored nearly as much as have their mechanical and chemical properties. Metals and various industrial plastics that are widely used for medical implants often lack the molecular sequence and patterns crucial for normal cell function, and can therefore trigger aberrant cell responses [6]. Therefore, more research investigating the link between chemical and physical surface properties and cellular cell response is important for future medical applications.

5.2. Materials and Methods

Micropatterned Polyurethane Preparation. Poly(ethylene glycol) (**PEG**, M_w=2,000, Sigma-Aldrich), poly(caprolactone) (**PCL** M_w=80,000, M_w/M_n=1.43,

Aldrich) solutions were prepared in chloroform ($CHCl_3$, Aldrich). PCL was selected at high molecular mass (M_w =80000) compared to the small PEG (M_w=2000) to reduce the end-to-end crosslinking of PCL-PCL and PCL-PEG. Therefore we expect two phases in the product: a PEG-rich polyurethane phase (that itself contains hard domains of MDI) and a PCL-rich uncrosslinked phase. The PEG/PCL composition-annealing temperature (• /T) two-dimensional libraries were prepared on 22 mm×22 mm silicon chips. Si was first treated with Piranha solutions (30 % hydrogen peroxide / 70 % sulfuric acid) for an hour at 80 ºC, then etched with Buffered Oxide Etchant **(BOE) 1:6**, JT Baker). Annealing temperature (80 to 120°C) and PCL composition (• $_{PCL}$, 0 to 0.3, mass fraction) gradients were generated along orthogonal directions using methods described previously [6, 31]. The PEG was chain-extended with 4,4 Methylene bis-phenyl diisocyanate (**MDI,** Sigma-Aldrich) and **Pluracol**® (a triol, Mw=430, BASF) in Tetrahydrofuran (**THF,** EMD). Driven by crystallization and LCST (lower critical solution temperature) phase separation mechanisms, PEG and PCL phases were separated to form specific surface phase patterns.

Cell Lines. Mouse osteoblasts (MC3T3-E1 subclone 4 from ATCC, Rockville, MD, passage 6 or 7) were used for this research for two reasons. From cellular biology, much previous research has made this a well-characterized model system [1,9,10,28]. For future applications of biomaterials, osteoblast growth and behavior is crucial to a wide range of orthopedic therapies.

Cell Culture and Assays. After sterilization (70% EtOH solution, 30 min), mouse osteoblast-like cells were seeded onto combinatorial chips of surface lateral patterns at a density of 5,000 cells/cm^2 and were cultured in DMEM with 10% fetal

bovine serum, L-glutamine and streptomycin at 37°C in a humidified 5% CO_2 atmosphere for 4 hours. Cell counter staining is done with Hoechst 33342 (Invitrogen). The MC3T3-E1 cell line was chosen based on previous experience culturing them on PCL, and based upon their ability to reproduce certain behaviors of normal mouse osteoblast [9].

Image Acquisition. Surface lateral patterns and cell density were studied by cross-polarized optical and fluorescent microscopy. These two different types of images were acquired sequentially over a grid of positions on each library by using a multi-channel microscope equipped with a robotic image acquisition system. Typically, for a 22mm×22mm library, at 10× magnification rate, 324 images from distinct locations (1,200• m×1000• m) were acquired. Quantitative descriptions of surface lateral patterns and cell proliferation were attained by image processing and analysis using ImageJ (NIH) and Matlab™ software.

Analysis. Quantitative descriptions of surface lateral patterns and cell proliferation were attained by image processing with ImageJ (NIH) and Matlab™. Six descriptors of PCL features were used: area, solidity, eccentricity, major axis length, minor axis length, and PCL-to-PCL spacing. Because these descriptors are not necessarily independent measures of pattern morphology, PCA [40] was used to reduce the dimensionality of the data. Briefly, the dataset was normalized followed by extraction of eigenvalues and eigenvectors from the singular value decomposition matrix of the normalized dataset. These eigenvalues were used to determine the minimum number of linearly-independent descriptors (eigenvectors) needed to describe at least 99% of the variance in the data.

Rotations are used to better align the directions of the factors with the original variables so that the factors may be more interpretable. We expect for clusters of variables that are highly correlated to define the rotated factors. The rotation's success at clustering the interpretability is highly dependent on the number of factors that you choose to rotate.

After the initial extraction, the factors are uncorrelated with each other. If the factors are rotated by an orthogonal transformation, such as varimax, the rotated factors are also uncorrelated. The varimax method tries to make elements of this matrix go toward 1 or 0 to show the clustering of variables.

5.3. Results and Discussion

The combinatorial library of surface lateral patterns covers a range of diverse shapes and sizes from circular islands only a few several microns in diameter to ribbon patterns nearly 70 μm long. The height of the features ranges from 0 to 1 μm. The results are shown in Figure 14. The bright areas shown under cross-polarized light are the crystalline PCL domains, while the amorphous PEG-rich background is shown as the dark area. PEG crystallization is suppressed due to formation of crosslinks in the polyurethane.

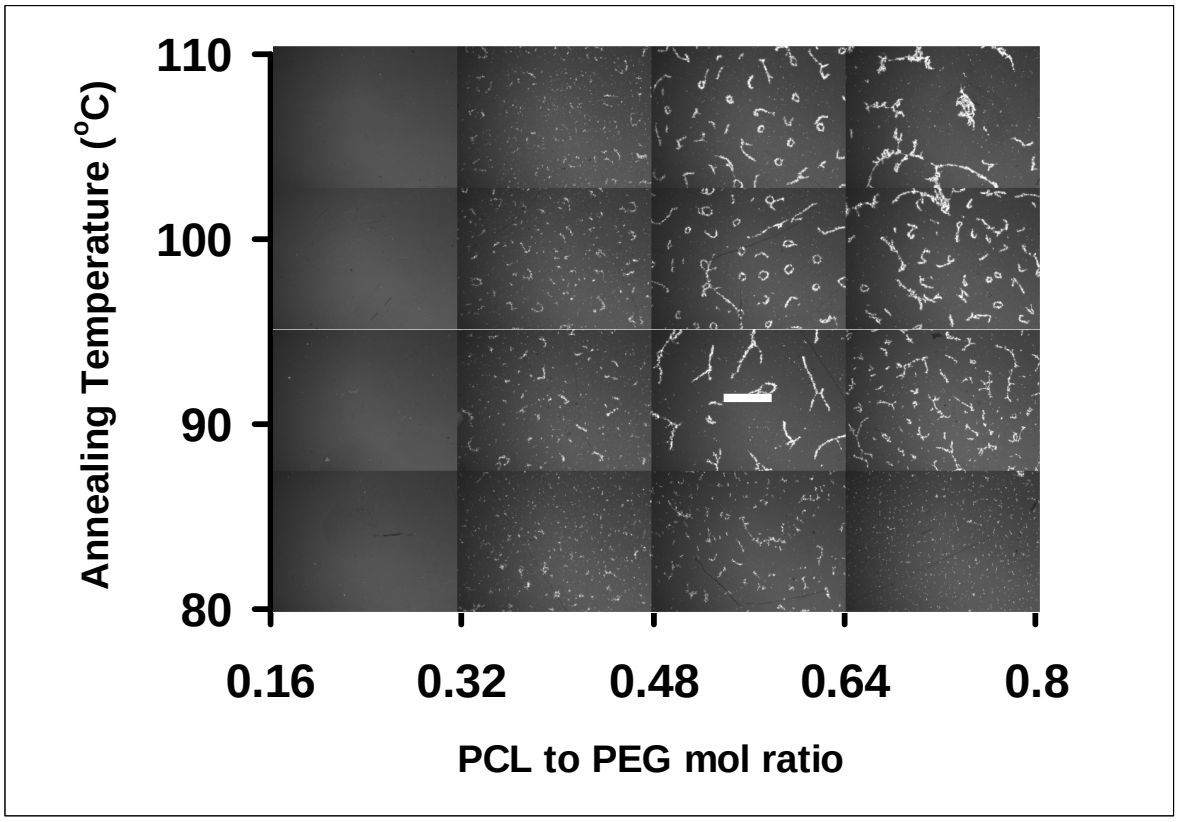

Figure 14. Combinatorial library of phase-separated features at different annealing temperature and PCL composition (10x magnification of cross-polarized image). *Bar: 300 • m.*

To illustrate the use of PCA to extract correlations information from the library, the subsequent images (Figure 15 and Figure 16) compare analysis using traditional one-to-one correlation of the pure parameters (Figure 15) and correlation between principal components from the dataset after rotation with Varimax method **(**details in Chapter 3) following PCA (Figure 16)).

Traditional one-to-one correlation between actual measured quantities for surface lateral patterns and subsequent cell culture, are shown in Figure 15.

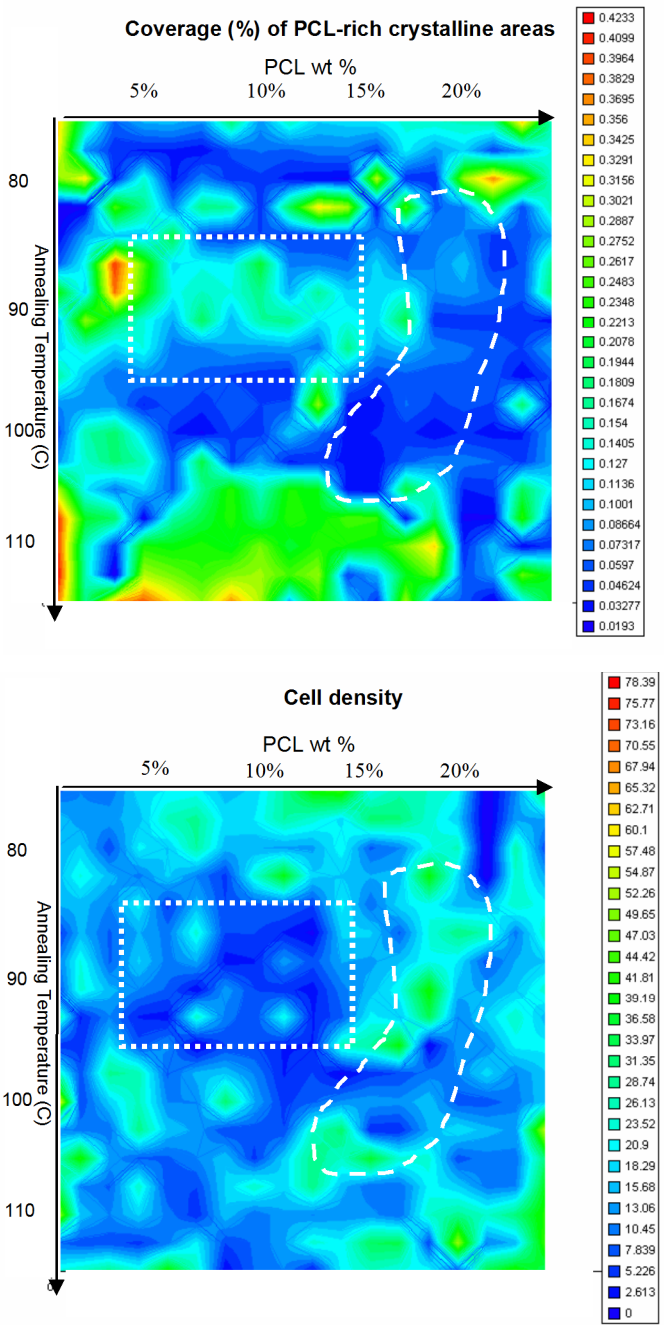

Figure 15. Results from image analysis of cells cultured on libraries. *Top:* Area coverage (%) of crystalline features. *Bottom:* Cell density (# of cells per 1.2 mm^2). Image is comprised of 324 data points from 22x22 mm library, each point being derived from 1,200 x 1,000 µm size image).

The image analysis results from cell culture grown on the library illustrated in Figure 14 are shown in Figure 15 (top) for the PCL feature size. Osteoblast density after

1 day of culture growth on the library is shown in Figure 15 (bottom). Note that the chosen surface metrics, area coverage of PCL and cell density, are plotted versus the actual library preparation variables, annealing temperature and PCL concentration. There is an apparent "negative" correlation between crystalline PCL area coverage and cell density. For example, within the rectangular boundaries in Figure 15, high crystalline area coverage corresponds to low cell density. In the oval boundaries in Figure 15, low crystalline area coverage corresponds to high cell density. However, there are regions where this negative correlation was not followed as well. The presentation of microstructural and cell-adhesive results as a function of library preparation conditions in Figure 15 is not a robust method for observing structure-function relationships. Rather, we desire direct knowledge of the correlation between cell density and the local microdomains surrounding cells. In particular, the consideration of % coverage of crystalline area probably overlooks other factors that influence cell function. This includes the 'local' distance between each cell and the neighboring PCL islands. This information cannot be captured by looking 'globally' at the variation of parameters over the library surface, as Figure 15 does. Further investigation into the details of the surface lateral patterns is needed so that we can better describe the cell-biomaterial interaction.

Therefore, the data from each image on the library in Figure 14 and the subsequent results from cell culture grown on it were analyzed with local cell-feature histograms (LCFH) [66,67,70], obtained by sorting various surface parameters and the cell density into bins. This approach offers several advantages: (1) the local interactions between cells and their immediate neighbors is considered, (2) the actual physical dimensions on the surface are illuminated, and (3) a wide range of surface feature

descriptors (anything that can be calculated from image analysis) can be used as independent variables. Figure 16 presents a LCFH analysis of the data from image analysis of cell culture grown on library depicted in Figure 14. Two candidate surface parameters are the area of a PCL-crystalline domain and its distance from each adherent cell. Figure 16 was constructed by sorting the distance between each cell and the PCL-crystalline features of a certain size, and counting the occurrences of each combination. The peaks in Figure 16 show that cells adhere preferably to certain combinations of distance and PCL size, and that other combinations are not preferable. This presentation, in terms of the local microstructural parameters surrounding each cell, allows a more direct exploration of the cell-surface relationships than Figure 15. However, in order to interpret LCFH correctly, one must consider the experimental results relative to random sampling, e.g., a random distribution of cells around the PCL islands will also produce certain distinct peaks. The ratio of the experimental to random reference histogram can be used to determine a probability distribution for cell attachment and to identify features that can act to influence, positively or negatively, cell attachment.

On PEG-MDI-Pluracol / PCL libraries novel PCL phases with ring-like morphology (Figure 16-insert) were discovered. Effects of PCL island size on cell attachment were analyzed and smaller PCL islands (Figure 16) were associated with increased cell attachment.

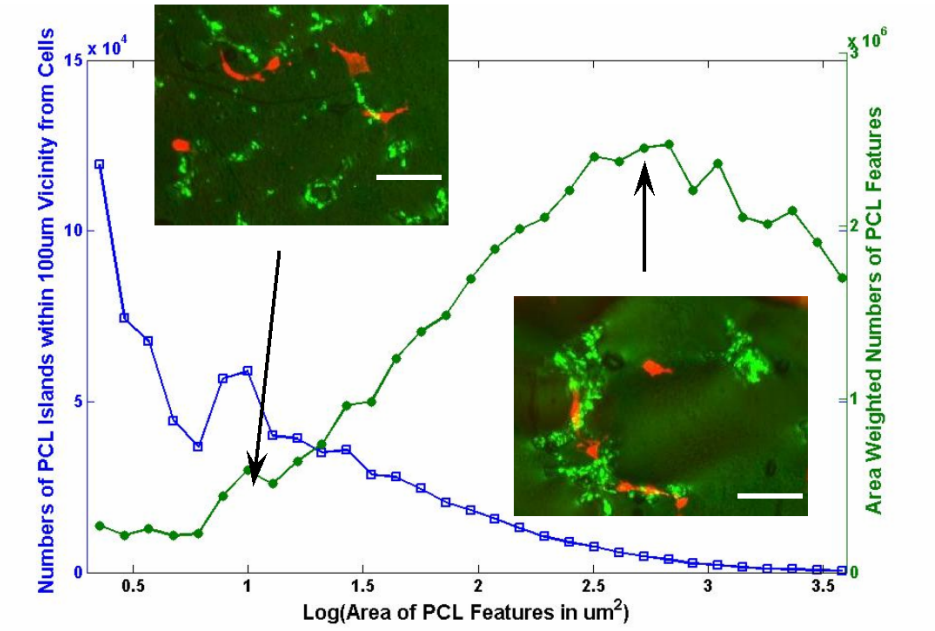

Figure 16. PCL feature size distribution (green solid circles) and cell attachment distribution on PEG-MDI-Pluracol/PCL Library (blue open squares). *Inserts:* Green=PCL phase; red= cell actin, bar = 100μm)

As shown in Figure 15 and Figure 16, changing focus from average to individual cell-surface pattern interaction opens up an opportunity to extract more information from the dataset. To further improve the efficiency of data analysis, PCA is employed to handle the complexities in the amount of data and potential artificial correlations between image metrics used.

PCA was used to analyze the quantitative data from image analysis of the patterned surfaces represented in Figure 14. Six parameters from surface pattern descriptor were examined: area, solidity, eccentricity, major diameter, minor diameter, and spacing. Spacing is defined as Euclidean distance between the center of mass of one feature to its closest neighbor. Five parameters from cellular adhesion response were examined: total number of cells captured in the same image, cell spreading area, cell perimeter, cell Feret diameter, and cell eccentricity. Briefly, the dataset was normalized

followed by extraction of eigenvalues and eigenvectors from the singular value decomposition matrix of the normalized dataset. These eigenvalues were used to determine the minimum number of linearly-independent descriptors (eigenvectors) needed to describe the variance in the data.

Table 8. Definitions of Eccentricity and Feret Diameter

Parameter	Definition	Illustration
Eccentricity (•)	$e = \sqrt{1 - \frac{b^2}{a^2}}$	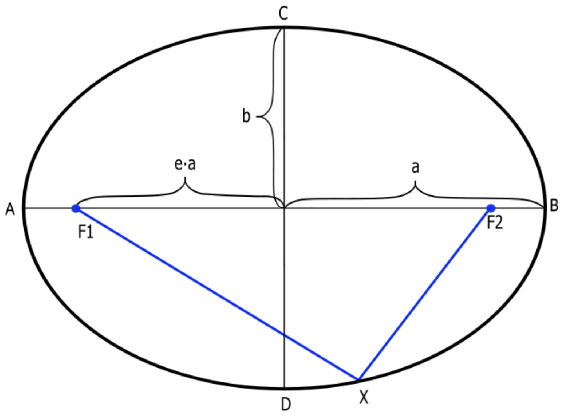
Feret Diameter	The longest distance between any two points along the selection boundary (also known as caliper length).	Feret Diameter of the ellipse above is the length of line AB.

Results from PCA on cellular responses are presented below in Table 9 and Figure 17, it is concluded that two PC is sufficient to explain the majority of variance in the data.

Table 9. Table of Eigenvalues for each Principal Component (PC) from PCA of cellular responses

Principal Components: on Correlations

Number	Eigenvalue	Percent	20 40 60 80	Cum Percent
1	3.4219	68.437		68.437
2	0.9914	19.827		88.265
3	0.3919	7.838		96.103
4	0.1590	3.180		99.283
5	0.0359	0.717		100.000

Table 10. Table of Eigenvectors for each Principal Component (PC) from PCA of cellular responses (each column represent each PC)

Eigenvectors

Cell#	-0.06059	0.99794	0.01817	-0.00965	-0.00485
Area	0.51051	0.02591	-0.06737	-0.80311	0.29865
Perimeter	0.52582	0.03356	-0.27259	0.05965	-0.80282
Feret	0.50468	0.04610	-0.41919	0.54919	0.51561
Ecc	0.45225	0.01400	0.86320	0.22306	0.02028

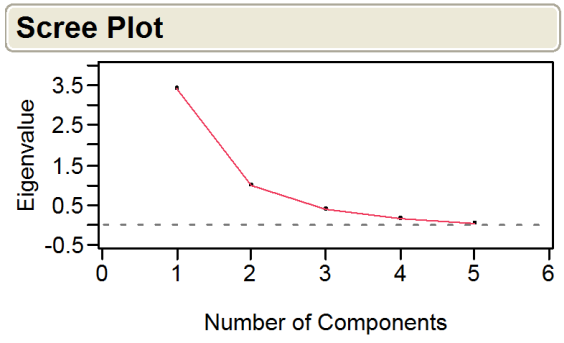

Figure 17. Scree plot of Eigenvalue of each PC

Results from Table 9 show that the first two PCs extracted with PCA contain all the parameters in the dataset. From the magnitude of eigenvectors in the first two PCs

presented in Table 10, cell spreading area (represented by area, perimeter, and feret diameter) and cell shape (represented by eccentricity) are the top dominant factors in the list, while the weaker one is the cell density (represented by number of cells captured within the same image at image acquisition). Further examination of descriptors of cell spreading (represented by area, perimeter, and feret diameter) showed strong correlations among themselves as illustrated in Figure 18.

Multivariate

Correlations

	Cell#	Area	Perimeter	Feret	Ecc
Cell#	1.0000	-0.0330	-0.0314	-0.0213	-0.0419
Area	-0.0330	1.0000	0.8995	0.8178	0.5732
Perimeter	-0.0314	0.8995	1.0000	0.9315	0.6163
Feret	-0.0213	0.8178	0.9315	1.0000	0.5854
Ecc	-0.0419	0.5732	0.6163	0.5854	1.0000

Scatterplot Matrix

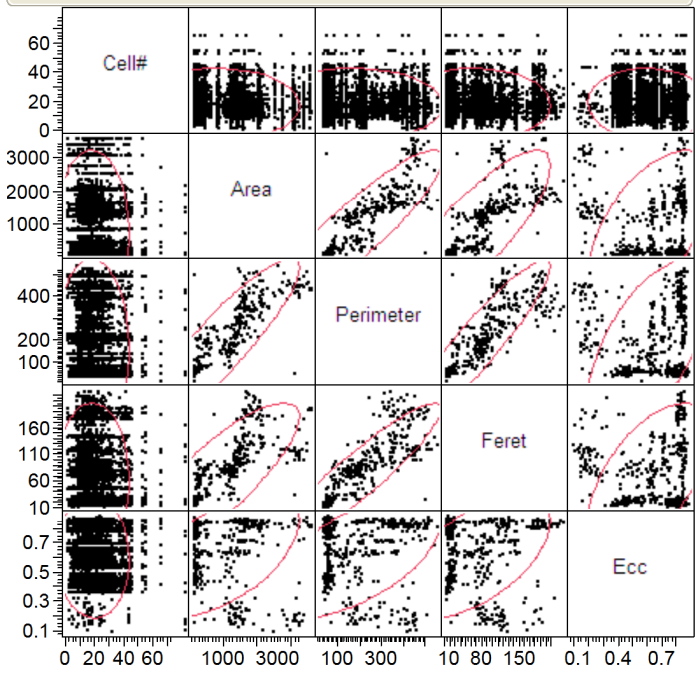

Figure 18. Correlations among cellular descriptors

K-means clustering is used to identify the presence of different states in the cells within the dataset. Briefly, the k-means approach is a special case of a general approach called the EM algorithm, where E stands for Expectation (the cluster means in this case) and the M stands for maximization, which means assigning points to closest clusters in this case. The optimum clustering is identified when optimum sum of distance is achieved with respect to the number of clusters.

The result from k-means clustering for cellular descriptors is illustrated in Figure 19 with color coding drawn on the scatterplot matrix to illustrate positions of the clusters with respect to the raw cellular data.

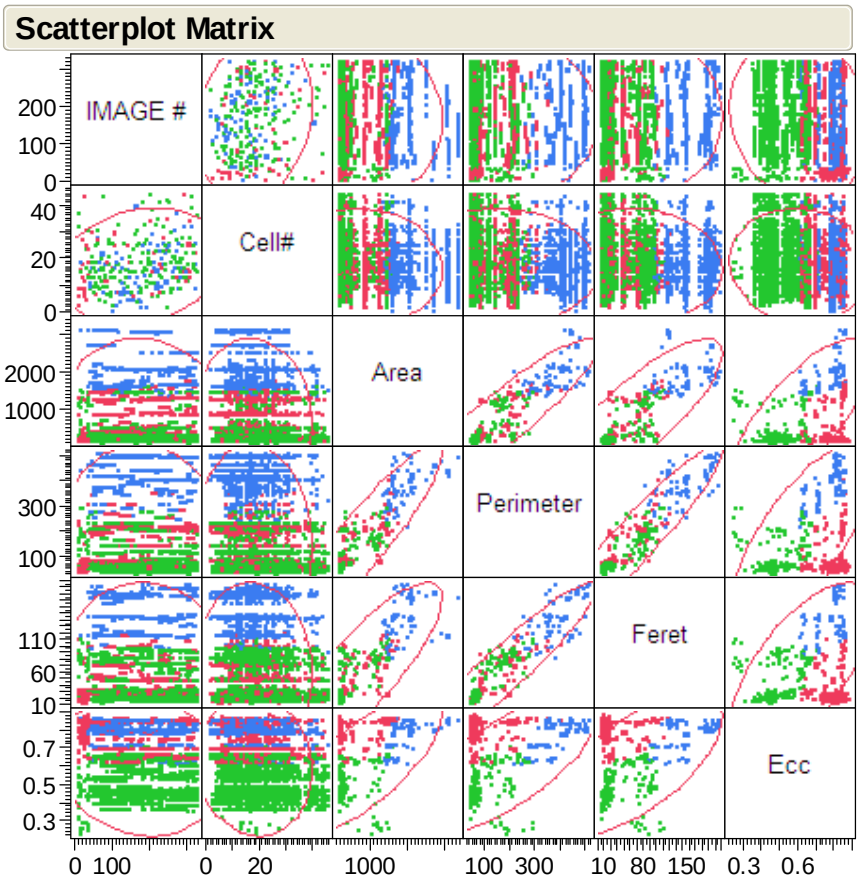

Figure 19. Results from k-means clustering reaching optimum at 3 clusters.
Legend: Cluster 1: Blue, Cluster 2: Green, Cluster 3: Red

The clustering result from cellular descriptors is as follow:

1. Green cluster: small cellular spreading, small eccentricity à small, circular cell (Cluster center: cell area 110, eccentricity 0.44)
2. Red cluster: small to medium cellular spreading, large eccentricity à small to medium, elongated cell (Cluster center: cell area 250, eccentricity 0.59)
3. Blue cluster: large cellular spreading, large eccentricity à large, elongated cell (Cluster center: cell area 1820, eccentricity 0.66)

The next step is to examine any correlations between the cellular descriptors to the surface pattern descriptors. The clustered properties from the cellular dataset are used to correlate to the clustered properties on the surface pattern dataset. Superimposing method is used to check on correlations between cluster assignment resulting from cellular descriptors and cluster assignment from surface pattern descriptor. Cluster labels from cellular descriptor clustering are superimposed (applied) to the surface patterns closest to each cell.

Briefly, each cell is correlated to the closest neighboring (or directly underneath) surface pattern, based on Euclidean distance between the center-of-mass of the cell to the center-of-mass of the surface pattern. Details on surface patterns descriptors were supplied in Chapter 4. Briefly, PCA was used to identify surface pattern area, spacing, solidity and eccentricity as the main surface descriptors, embedded in the three PCs identified from PCA. Those three surface descriptor PCs, containing the four surface descriptors, are rotated with Varimax method (details explained in Chapter 3) to yield orthogonal factors to enhance visualization of the clustering. The resulting clustering in surface pattern descriptor is illustrated in Figure 20.

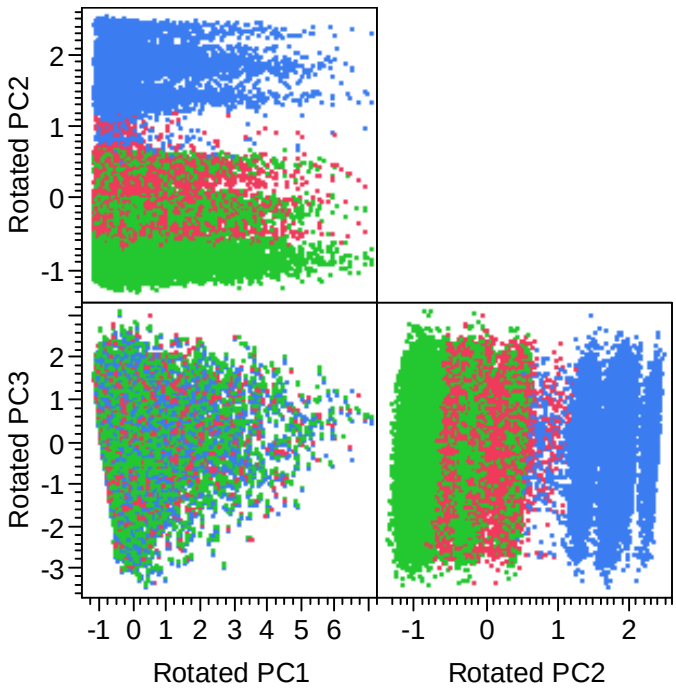

Figure 20. Scatterplot Matrix of PC1, PC2, and PC3 of surface pattern descriptors after Varimax Rotation (details of Varimax was explained in Chapter 3)

Figure 20 shows that clustering labels in cellular responses corresponds to clustering in surface pattern descriptors, as well. PC1 contains spacing, while PC2 and PC3 contain eccentricity and solidity, of surface pattern descriptors – PC2 is dominated by eccentricity, while PC3 is dominated by solidity (Table 5). Correlation between surface pattern descriptors to cellular descriptors is inferred from the co-location of each cluster assignments from cellular descriptors when superimposed on surface pattern descriptors. Figure 20 above provides the following observations:

1. Green cellular descriptor cluster (small, circular cells) co-locates with low PC2 (small eccentricity) from surface pattern descriptor à small, circular cells co-locates with circular surface pattern

2. Red cellular descriptor cluster (small-to-medium, elongated cells) co-locates with medium PC2 (medium eccentricity) from surface pattern descriptor à small-to-medium, elongated cells co-locates with moderately elongated surface pattern
3. Blue cellular descriptor cluster (large, elongated cells) co-locates with high PC2 (large eccentricity) from surface pattern descriptor à large, elongated cells co-locates with elongated surface pattern.

Certain cellular size and shape is known to indicate specific cellular state [9]; for example: small and circular cells indicate apoptotic cells, while large, spread out cells indicate live and growing cells. The findings and comments on the correlation between cellular descriptors and surface pattern descriptors, were summarized in the first four columns in Table 11 (Note: the comments on some possible related cellular states were solely based on inference from cell size and shape).

Visualization of cellular descriptor clustering is represented in the following Figure 21.

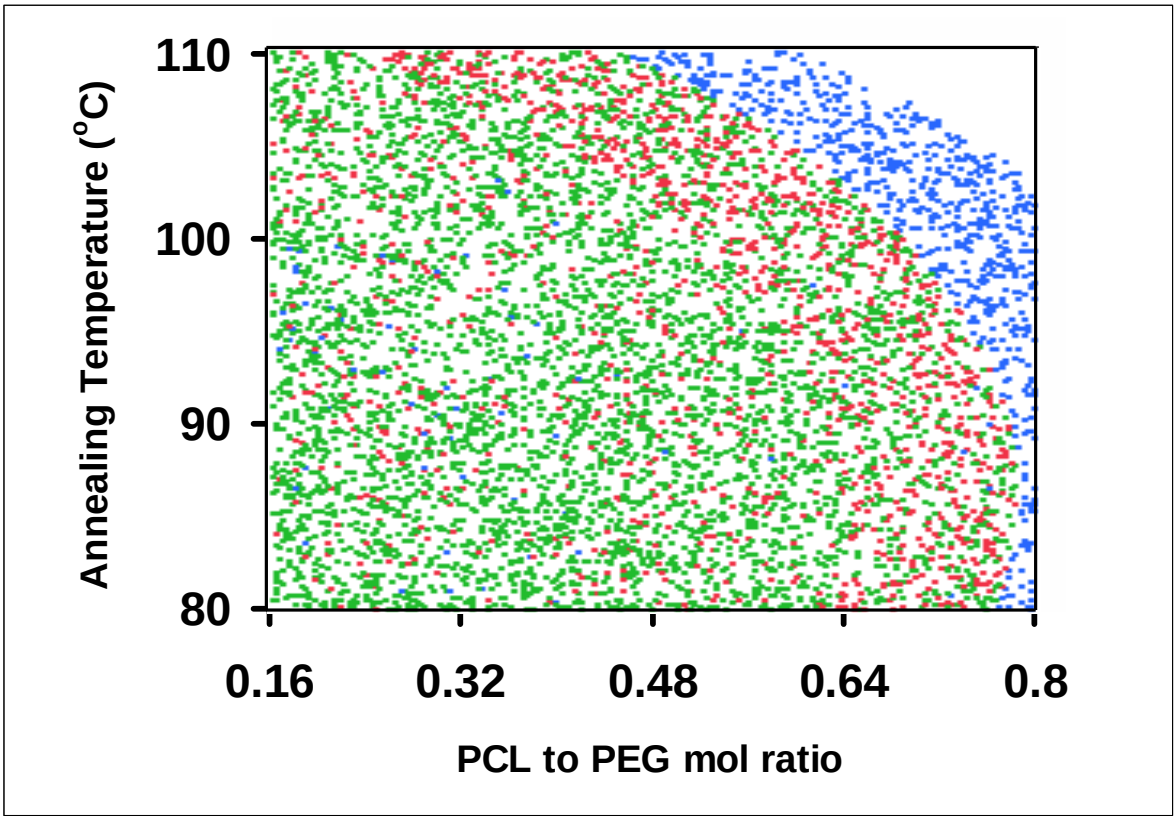

Figure 21. Superimposed clustering result based on cellular descriptors on original (T,•) surface pattern library

The chains of correlations from cellular response back to the surface descriptors show correlation between surface pattern descriptors and the subsequent cellular adhesion responses. Applying the color code to data from Table 3 above, cluster centers from the three clusters presented in Figure 19 indicate three different modes from the dataset. Taking the clustering results (color coded) and applying the cluster designation (presented in Figure 19) to surface descriptor data (presented in Figure 12 and Table 6) yielded the summary presented in Table 11.

Table 11. Analysis on cellular response clustering and correlation between cellular response to surface pattern size and shape. *Bar: 5 • m.*

Inferred Cellular State[9]	**Area (• m^2)**	**Eccentricity**	**Illustration**	**Color Code**	**Surface PC1 (dominant factor: spacing)**	**Surface PC2 (dominant factor: eccentricity)**
Apoptotic cells	Small (110 +/- 60)	Small (0.44+-0.23)	Small area, circular cells 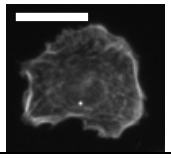	Green	Low	Low (circular pattern)
Undetermined-state cells	Small to medium (250+-50)	Large (0.59+-0.58)	Moderate area, elongated cells 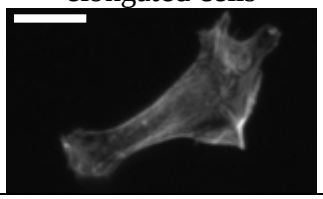	Red	Low	Medium (i.e. worm-like pattern)
Live cells	Large (1820+-610)	Large (0.66+-0.32)	Large area, elongated cells 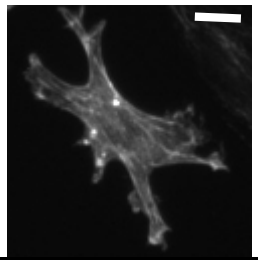	Blue	Low	High (elongated pattern)

Table 11 shows that specific spacings are favored upon adhesion. Namely cells show preference to adhere close to or on surface patterns. Furthermore, certain pattern shapes are correlated to certain cellular states, e.g. circular patterns favors small, circular cells, while elongated patterns favor large, elongated cells. This is in line with previous studies from Chen et al., who studied geometric control of cell life and death, and found that certain area and spacing of adhesive patterns induced certain cell adhesion areas and

cellular states [9]. Solid, circular adhesive patterns were correlated to small, circular spreading area on adhered cells, and this was correlated to apoptotic cell state. However, the effect of surface pattern's solidity does not show any conclusive trend in this dataset. This might be due to the existence of correlation between solidity and eccentricity as described in Chapter 1. Further study is needed to examine the causal relationship and getting confirmation on the exact mechanism of perception from the cells toward the surface patterns.

5.4. Conclusions and Future Directions

Correlation is observed between surface pattern descriptors and the subsequent cellular adhesion responses. Certain spacing in surface pattern is favored for cell adhesion: i.e. cells shows preference to adhere close to or on surface patterns. Furthermore, certain shapes are correlated to certain cellular states, i.e. circular pattern favors apoptotic cells, while elongated patterns favor viable cells. However, the effect of surface pattern's solidity and area did not show any conclusive trend in this dataset. This might be due to the existence of correlation between solidity and eccentricity as described in Chapter 1. Further improvement in the surface pattern library generation is necessary for future studies.

Research in the field of cellular study with the ultimate goal to tune cellular responses via signals from surface cues will need an examination of a causal relationship beyond this observed correlation between surface patterns and cellular adhesion responses. More specifically, confirmatory study on the exact mechanism of perception from the cells toward the surface patterns is necessary. This study accomplishes the goal

to demonstrate the efficient screening and exploration of vast and complex dataset, extracting important and meaningful information to narrow down the future path of study in this field.

5.5. References

1. Meredith, J.C., et al., *Combinatorial characterization of cell interactions with polymer surfaces.* J Biomed Mater Res, 2003. **66A**(3): p. 483-90.
2. Brocchini, S., K. James, V. Tangpasuthadol, and J. Kohn, *A combinatorial approach for polymer design.* J. Amer. Chem. Soc., 1997. **119**(19): p. 4553-4554.
3. Brocchini, S., et al., *Structure-property correlations in a combinatorial library of degradable biomaterials.* J Biomed Mater Res, 1998. **42**(1): p. 66-75.
4. B. J. Spargo, e.a., *Spatially controlled adhesion, spreading, and differentiation of endothelial cells on self-assembled molecular monolayer.* Proc. Nat. Acad. Sci, 1994. **91**: p. 11070-11074.
5. C. S. Ranucci, P.V.M., *Polymer Substrate topography actively regulates the multicellular organization and liver-specific functions of cultured hepatocytes.* Tissue Eng., 1999. **5**: p. 407-420.
6. Evangelos Tziampazis, J.K., Prabhas V. Moghe, *PEG-variant biomaterials as selectively adhesive protein templates: model surfaces for controlled cell adhesion and migration.* Biomaterials, 2000. **21**: p. 511-520.
7. Ratner BD, C.D., Horbett TA, Lenk TJ, Lewis KB, Rapoza RJ, *Biomolecular and Surfaces.* Vac. Sci. Technol. A., 1990. **8**(3): p. 2306-2317.
8. Sarikaya, M., et al., *Molecular biomimetics: nanotechnology through biology.* Nat Mater, 2003. **2**(9): p. 577-85.
9. Christopher S. Chen, e.a., *Geometric control of cell life and death.* Science, 1997. **276**(5317): p. 1425-1428.
10. Chen, G., Y. Imanishi, and Y. Ito, *Effect of protein and cell behavior on pattern-grafted thermoresponsive polymer.* J Biomed Mater Res, 1998. **42**(1): p. 38-44.
11. A. Garcia, P.D., D. Boettiger, *The effect of surface reaction stage on fibronectin-mediated adhesion of osteoblast-like cells to bioactive glass.* J. Biomed. Mater. Res., 1998. **40**: p. 48-56.
12. A. Garcia, P.D., D. Boettiger, *Modulation of cell proliferation and differentiation trhough substrate-dependent changes in fibronectin conformation.* Mol. Biol. Cell, 1999. **10**: p. 785-798.
13. Braun, R., M. Sarikaya, and K. Schulten, *Genetically engineered gold-binding polypeptides: structure prediction and molecular dynamics.* J Biomater Sci Polym Ed, 2002. **13**(7): p. 747-57.
14. Bruggemann, O., *Molecularly imprinted materials--receptors more durable than nature can provide.* Adv Biochem Eng Biotechnol, 2002. **76**: p. 127-63.

15. S. Huang, D.I., *Shape-dependent control of cell growth, differentiation, and apoptosis: Switching between attactors in cell regulatory network.* Exp. Cell. Res., 2000. **261**: p. 91-103.
16. D. Itoh, S.Y., S. Kuroda, H. Kondo, A. Umezawa, K. Ohya, . Ohyama, S. Kasugai, *Enhancement of osteogenesis on hydroxyapatite surface coated with synthetic peptide (EEEEEEEPRGDT) in vitro.* 2002: p. 292-297.
17. D.H. Davis, C.S.G., R.W. Johnson, T.A. Desai, *Immobilization of RGD to <111> silicon surfaces for enhanced cell adhesion and proliferation.* Biomaterials, 2002. **23**: p. 4019-4027.
18. Kao, W.J., *Evaluation of protein-modulated macrophage behavior on biomaterials: designing biomimetic materials for cellular engineering.* Biomaterials, 1999. **20**: p. 2213-2221.
19. L. Kam, W.S., J. N. Turner, R. Bizios, *Selective adhesion of astrocytes to surfaces modified with immobilized peptides.* Biomaterials, 2002. **23**: p. 511-515.
20. M. C. Porte-Durrieu, C.L., F. Villars, F. Lefebvre, S. Dutoya, A. Guette, L. Bordenave, C. Baquey, *Development of RGD peptides grafted onto silica surfaces: XPS characterization and human endothelial cell interaction.* 1999: p. 368-375.
21. P. Banerjee, D.J.I., A.M. Mayes, L.G. Griffith, *Polymer latexes for cell-resistant and cell-interactive surfaces.* 2000.
22. S.P. Massia, J.S., *Immobilized RGD peptides on surface-grafted dextran promote biospecific cell attachment.* 2001: p. 390-399.
23. Chen CS, e.a., *Cell Shape provides global control of focal adhesion assembly.* Biochemical and Biophysical Research Communication, 2003. **307**: p. 355-361.
24. John l. Tan, J.T., Dana M. Pirone, Darren S. Gray, Kiran Bhadriraju, Christopher S. Chen, *Cells lying on a bed of microneedles: An approach to isolate mechanical force.* PNAS, 2003. **100**(4): p. 1484-1489.
25. Gray DS, T.J., Chen CS, *Repositioning of cells by mechanotaxis on surfaces with micropatterned Young's modulus.* Journal of Biomedical Material Research, 2003. **66A**: p. 605-614.
26. Y. W. Fan, F.Z.C., L.N.Chen, Y. Zhai, Q.Y. Xu, I-S. Lee, *Adhesion of neural cells on silicon wafer with nano-topographic surface.* Applied Surface Science, 2002. **2002**(187): p. 313-318.
27. Hirokaju Kaji, e.a., *Microelectrochemical Approach to Induce Local Cell Adhesion and Growth on Substrates.* 2004. **20**: p. 16-19.
28. B. D. Boyan, T.W.H., D. D. Dean, Z. Schwartz, *Role of material surfaces in regulating bone and cartilage cell response.* Biomaterials, 1996. **17**: p. 137-146.
29. E. Ostuni, C.S.C., D.E. Ingber, G.M. Whitesides, *Selective Deposition of Proteins and Cells in Arrays of Microwells.* Langmuir, 2001. **17**: p. 2828-2834.
30. Gray, D.S., J. Tien, and C.S. Chen, *Repositioning of cells by mechanotaxis on surfaces with micropatterned Young's modulus.* J Biomed Mater Res, 2003. **66A**(3): p. 605-14.
31. Tan, J.L., et al., *Cells lying on a bed of microneedles: an approach to isolate mechanical force.* Proc Natl Acad Sci U S A, 2003. **100**(4): p. 1484-9.

32. E. Ostuni, R.K., C.S. Chen, D.E. Ingber, G.M. Whitesides, *Patterning Mammalian cells Using Elastomeric Membranes.* Langmuir, 2000. **16**: p. 7811-7819.
33. Wójciak-Stothard B, M.Z., Korohoda W, Curtis A and Wilkinson C, *Activation of macrophage-like cells by multiple grooved substrata:Topographical control of cell behavior.* Cell Biology International, 1995. **19**: p. 485-490.
34. Folkman J, M.A., *Role of cell shape in growth control.* Nature, 1978. **273**: p. 345-349.
35. Chicurel ME , C.S., Ingber DE, *Celular control lies in the balance of forces.* Current Opinion in Cell Biology, 1998. **10**: p. 232-239.
36. Weber, N., et al., *Small changes in the polymer structure influence the adsorption behavior of fibrinogen on polymer surfaces: validation of a new rapid screening technique.* J Biomed Mater Res, 2004. **68A**(3): p. 496-503.
37. Schachter, D.M.a.J.K., *A synthetic polymer matrix for the delayed or pulsatile release of water-soluble peptides.* J. Control. Rel, 2002. **78**: p. 143-153.
38. Yu, C., S.S. Mielewczyk, K.J. Breslauer, and J. Kohn, *Tyrosine-PEG-derived poly(ether carbonate)s as new biomaterials. Part II: Study of inverse temperature transitions.* Biomaterials, 1999. **20**(3): p. 265-272.
39. Yu, C.a.J.K., *Tyrosine-PEG-derived poly(ether carbonate)s as new biomaterials. Part I: Synthesis and Evaluation.* Biomaterials, 1999. **20**(3): p. 253-264.
40. Tangpasuthadol, V., S.M. Pendharkar, and J. Kohn, *Hydrolytic degradation of tyrosine-derived polycarbonates, a class of new biomaterials. Part I: Study of model compounds.* Biomaterials, 2000. **21**: p. 2371-2378.
41. Jack R. Smith, A.S., Norbert Weber, Doyle Knight, Sascha Abramson, Joachim Kohn, *Integration of Combinatorial Synthesis, Rapid Screening, and Computational Modeling in Biomaterial Development.* Macromolecules Rapid Communication, 2004. **25**: p. 127-140.
42. J.C. Meredith, E.J.A., *LCST Phase Separation in Biodegradable Polymer Blends: poly(D,L-lactide) and poly(sigma-caprolactone).* Macromolecules Chemical Physics, 2000. **201**: p. 733-739.
43. Muhammed A. Al-Nasassrah, F.P., J. Michael Newton, *The effect of an increase in chain length on the mechanical properties of polyethylene glycols.* European Journal of Pharmaeutics and Biopharmaeutics, 1998. **46**: p. 31-38.
44. Faucheux, N.S., R.; Lutzow, K.; Werner, C.; Groth, T., *elf-assembled monolayers with different terminating groups as model substrates for cell adhesion studies.* Biomaterials, 2004. **25**(14): p. 2721-2730.
45. Emanuele Ostuni, B.A.G., Milan Mrksich, Carmichael S. Roberts, George M. Whitesides, *Adsorption of Proteins into Hydrophobic Sites on Mixed Self-Assembled Monolayers.* Langmuir, 2003. **19**: p. 1861-1872.
46. Alves, C.M.R., R. L.; Hunt, J. A., *Preliminary study on human protein adsorption and leukocyte adhesion to starch-based biomaterials.* Journal of Materials Science: Materials in Medicine, 2003. **14**(2): p. 157-165.
47. C.M. Nelson, S.R., J.L. Tan, C.S. Chen, *Degradation of Micropatterned Surfaces by Cell-dependent and Independent Processes.* Langmuir, 2003. **19**: p. 1493-1499.

48. Schauer, T.E., Claus D, *Organic polymer treatment - the way to modern pigments.* European Coatings Journal, 2003. **3**: p. 114-120.
49. J. Brandup, E.H.I., and E.A. Grulke; associate editors, A. Abe, D.R. Bloch., *Polymer Handbook.* 1999. **4**.
50. Tadakoro, H., *Structure and properties of crystalline polymers.* Polymer, 1984. **25**(2): p. 147-164.
51. Wenbing Hu, V.B.F.M., *Liquid-liquid demixing in binary polymer blend driven solely by the component-selective crystallizability.* Journal of Chemical Physics, 2003. **119**(20): p. 10953-10957.
52. M. Doytcheva, D.D., R. Stamenova, C. Tsvetanov, *UV-initiated crosslinking of Poly(ethylene oxide) with pentaerythritol Triacrylate in solid state.* Macromolecules Material Engineering, 2001. **286**(1): p. 30-33.
53. Haugland, R.P., *Handbook of Fluorescent Probes and Research Products.* 2002. **9th Edition**: p. 461.
54. Kovacs, A.J.G., A.; Straupe, C.*] Isothermal growth, thickening, and melting of poly(ethylene oxide) single crystals in the bulk.* Journal of Polymer Science, 1974. **50**: p. 283-325.
55. G Natta, I.W.B., G. Allegra, Acc. Naz. Lincei Rend, 1961. **31**: p. 350.
56. D.A. Winesett, S.S., J. Luning, H. Ade, *Tuning substrate surface energies for blends of polystyrene and poly(mthyl methacrylate).* Langmuir, 2003. **19**: p. 8526-8535.
57. Orban, J.M.C., Toby M.; Wagner, William R.; Jankowski, Ron., *Easily grafted polyurethanes with reactive main chain functional groups. Synthesis, characterization, and antithrombogenicity of poly(ethylene glycol)-grafted poly(urethanes).* Journal of Polymer Science, Part A: Polymer Chemistry, 1999. **37**(17): p. 3441-3448.
58. Henn, G.S., M.; Poths, H.; Ruecker, M.; Rabe, J. P., *Influence of order in thin smectic polymer films on the structure at the surface.* Physica B: Condensed Matter (Amsterdam), 1996. **221**(1-4): p. 174-184.
59. Doye, J.P.K., *Computer simulations of the mechanism of thickness selection in polymer crystals.* Polymer, 2000. **41**(25): p. 8857-8867.
60. Chattopadhyay, S.M., J. Carson, *Instability and dewetting of conducting-insulating polymer thin-film bilayers.* Macromolecular Rapid Communications, 2004. **25**(1): p. 275-279.
61. Patel, N., et al., *Printing patterns of biospecifically-adsorbed protein.* J Biomater Sci Polym Ed, 2000. **11**(3): p. 319-31.
62. A. El-Ghannam, L.S., J. Jones, *Laminin-5 coating enhances epithelial cell attachment, spreading, and hesmidesmosome assembly on Ti-6Al-4V implant material in vitro.* J. Biomed. Mater. Res., 1999. **41**: p. 30-40.
63. A. El-Ghannam, P.D., I. M. Shapiro, *effect of serum proteins on osteoblast adhesion to surface-modified bioactive glass and hydroxyapatite.* J. Orthopaed. Res., 1999. **17**: p. 340-345.
64. Aaron S. Goldstein, P.A.D., *Effect of adsorbed fibronectin concentration on cell adhesion and deformation under shear on hydrophobic surfaces.* Journal of Biomedical Material Research, 2002. **59**(4): p. 665-675.
65. Bruce Albert, e.a., *Molecular Biology of the Cell.* 2002. **4th Edition**.

66. Su, Jing, Zapata, Pedro, Meredith, J. Carson, *Knowledge discovery applications in high-throughput polymer characterization,* Materials Research Society Symposium Proceedings, 2006, 894.
67. Su, Jing, Meredith, Carson, *Knowledge discovery applications in combinatorial biomaterial surface design.* PMSE Preprints, 2005. **93**: p 1049.
68. Bailey, LeeAnn, et al. *Cellular Response to Phase-separated Blends of Tyrosine-derived Polycarbonates,* J. Biomed Mat Res A, 2006. **76a**(3): p. 491.
69. Kholodovych, Vladyslav, et al. *Accurate predictions of cellular response using GSPR: a feasibility test of rational design of polymeric biomaterial,* Polymer, 2004. **23**: p 7367-7379.
70. Su, J., Zapata, P., and J.C. Meredith, *Local Cell Feature Metrics: A Novel Method for Analysis of Cell-Cell Interactions,* BMC Bioinformatics, 2009, accepted.

CHAPTER 6

SUMMARY AND RECOMMENDATIONS

6.1. Summary

PCL-rich features exhibiting a variety of shapes, sizes, and spacings within a PEG-rich phase background was obtained from high-throughput screening of combinatorial libraries in material composition and processing temperature. PCL-rich phase shapes observed included 'rings', 'chains', and 'worms'. Deconvolution of the control of spacing, size, and shape of PCL features was achieved by varying the composition of MDI, the tri-functional chain extender Pluracol, the PCL content, and the annealing temperature. Optimum composition and annealing temperature to achieve minimum weight loss upon immersion into aqueous solution (~ 1 d), and desired visual contrast between surface patterns and background, are achieved at 34% MDI mole excess with respect to PEG, between 40-70% mole ratio of Pluracol to PEG, and at annealing temperature of ~ 110^{o} C. The ability to generate the library with different ratio of adhesive-vs-non-adhesive area within the surface pattern, as well as the effect of shape, orientation, area, and spacing will play an important role for further cellular response studies focusing on effect of surface physical cues on adherent cells.

Correlation is observed between surface pattern descriptors and the subsequent cellular adhesion responses. Certain spacing in surface pattern is favored for cell adhesion: i.e. cells shows preference to adhere close to or on surface patterns. Furthermore, certain shapes are correlated to certain cellular states, i.e. circular pattern

favors apoptotic cells, while elongated patterns favor viable cells. However, the effect of surface pattern's solidity and area did not show any conclusive trend in this dataset. This might be due to the existence of correlation between solidity and eccentricity as described in Chapter 1.

This study accomplishes the goal to demonstrate the efficient screening and exploration of vast and complex dataset, extracting important and meaningful information to be used in future studies. Possible further studies on the current results on cell-to-surface pattern correlation include surface design to grow functional cells/tissues.

In general, potential applications to the new method of generating surface pattern library include structure-property understanding of co-polymers or polymer blend (doped polymer) behavior, such as coating adhesion or surface tear-resistance. Applications of the HTS are virtually on every new exploration of new, multi-parameter problems, where resources are limited.

6.2. Recommendations

Further improvement in the surface pattern library generation is necessary for future studies to enable a full deconvolution of spacing, size, and shape. Research in the field of cellular study with the ultimate goal to tune cellular responses via signals from surface cues will need an examination of a causal relationship beyond these observed correlations between surface patterns and cellular adhesion responses. More specifically, confirmatory study on the exact mechanism of perception from the cells toward the surface patterns is necessary.

Co-staining protocols enhancement will be needed to enable high-throughput image acquisition in one-step imaging. It is desired to get cell functions and/or key

proteins staining, such as BrDU, vinculin and/or vitronectin, to be achieved on the same combinatorial chip with the surface pattern imaging in order for correlational studies from surface patterns to cellular states to be possible.

6.3. References

1. Aamer, Khaled A., et al *Development of high- throughput combinatorial screening method for probing cell-biomaterials interactions.* PMSE Preprints (2008), 98 838-839.
2. Harris, Nicole, et al. *Rapid discovery of biologically relevant polymer properties: from concept to validation.* PMSE Preprints (2006), 95 1039-1040.
3. Smith, Jack R, et al. *Integration of combinatorial synthesis, rapid screening, and computational modeling in biomaterials development.* Macromolecular Rapid Communications (2004), 25(1), 127-140
4. Treiser Matthew D, et al. *Profiling cell-biomaterial interactions via cell-based fluororeporter imaging.* BioTechniques (2007), 43(3), 361-6, 368.
5. Kohn Joachim, et al. *A new approach to the rationale discovery of polymeric biomaterials.* Biomaterials (2007), 28(29), 4171-7.